AD-A050 020 NAVAL POSTGRADUATE SCHOOL MONTEREY CALIF F/G 9/1
EXPERIMENTAL INVESTIGATION OF THE EFFECTS OF FLUID LOADING ON F--ETC(U)
DEC 77 J L JARVIS

UNCLASSIFIED NL

| OF |
AD
A050020

END
DATE
FILMED
3-78
DDC

(2)
NW

NAVAL POSTGRADUATE SCHOOL
Monterey, California

THESIS

EXPERIMENTAL INVESTIGATION OF THE EFFECTS OF FLUID LOADING ON FLEXURAL WAVES IN PLATES

by

James Laing Jarvis

December 1977

Thesis Advisor: O. B. Wilson

UNCLASSIFIED

SECURITY CLASSIFICATION OF THIS PAGE (When Data Entered)

REPORT DOCUMENTATION PAGE	READ INSTRUCTIONS BEFORE COMPLETING FORM
1. REPORT NUMBER	2. GOVT ACCESSION NO. / 3. RECIPIENT'S CATALOG NUMBER (19)
4. TITLE (and Subtitle) (6) Experimental Investigation of the Effects of Fluid Loading on Flexural Waves in Plates,	5. TYPE OF REPORT & PERIOD COVERED Master's Thesis; December 1977 / 6. PERFORMING ORG. REPORT NUMBER
7. AUTHOR(s) (10) James Laing Jarvis	8. CONTRACT OR GRANT NUMBER(s)
9. PERFORMING ORGANIZATION NAME AND ADDRESS Naval Postgraduate School Monterey, California 93940	10. PROGRAM ELEMENT, PROJECT, TASK AREA & WORK UNIT NUMBERS
11. CONTROLLING OFFICE NAME AND ADDRESS Naval Postgraduate School Monterey, California 93940 (11)	12. REPORT DATE Dec[illegible]77 / 13. NUMBER OF PAGES
14. MONITORING AGENCY NAME & ADDRESS(if different from Controlling Office) Naval Postgraduate School Monterey, California 93940 (12) 69 p.	15. SECURITY CLASS. (of this report) Unclassified / 15a. DECLASSIFICATION/DOWNGRADING SCHEDULE

16. DISTRIBUTION STATEMENT (of this Report)

Approved for public release; distribution unlimited

17. DISTRIBUTION STATEMENT (of the abstract entered in Block 20, if different from Report)

18. SUPPLEMENTARY NOTES

19. KEY WORDS (Continue on reverse side if necessary and identify by block number)

Flexural Disk Transducer
Flexural Waves in Plates

20. ABSTRACT (Continue on reverse side if necessary and identify by block number)

An experimental investigation was conducted of the effects of fluid loading on axially symmetric flexural waves in a circular aluminum plate 25 in. in diameter and 5/16 in. thick. Measurements were made of the flexural wavelength and natural frequencies with the plate in air, and with water loading on one side, over a frequency range from 20 kHz to 80 kHz. The critical (coincidence) frequency, that frequency at which the

DD FORM 1 JAN 73 1473 (Page 1) EDITION OF 1 NOV 65 IS OBSOLETE S/N 0102-014-6601

UNCLASSIFIED

SECURITY CLASSIFICATION OF THIS PAGE (When Data Entered)

251450

speed of the flexural wave equals the speed of sound in water, occurs at approximately 45 kHz. The measured flexural-wave speeds with air loading are in good agreement with theory. With water loading, the wave speed decreases, the amount of decrease increasing to approximately 14 percent below the in-air value just below the critical frequency. At the critical frequency, the wave speed appears to jump to values nearly equal to the unloaded values. Radiation patterns were obtained and when edge effects are eliminated, are in qualitative agreement with theoretical predictions for an infinite fluid-loaded plate.

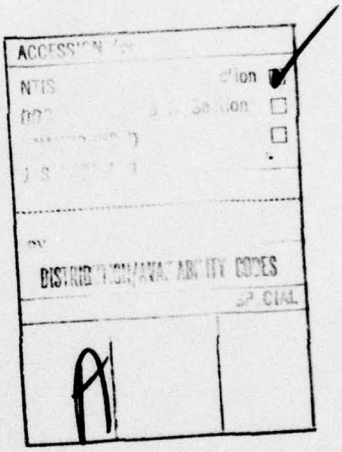

Approved for public release; distribution unlimited

Experimental Investigation of the Effects of Fluid Loading on Flexural Waves in Plates

by

James Laing Jarvis
Lieutenant, United States Navy
B.S.B.A., University of Florida, 1968

Submitted in partial fulfillment of the requirements for the degree of

MASTER OF SCIENCE IN ENGINEERING ACOUSTICS

from the

NAVAL POSTGRADUATE SCHOOL

December 1977

Author: James J. Jarvis

Approved by: O B Wilson
Thesis Advisor

James V. Sanders
Second Reader

Chairman, Department of Physics and Chemistry

George J. Haltiner
Dean of Science and Engineering

ABSTRACT

An experimental investigation was conducted of the effects of fluid loading on axially symmetric flexural waves in a circular aluminum plate 25 in. in diameter and 5/16 in. thick. Measurements were made of the flexural wavelength and natural frequencies with the plate in air, and with water loading on one side, over a frequency range from 20 kHz to 80 kHz. The critical (coincidence) frequency, that frequency at which the speed of the flexural wave equals the speed of sound in water, occurs at approximately 45 kHz. The measured flexural-wave speeds with air loading are in good agreement with theory. With water loading, the wave speed decreases, the amount of decrease increasing to approximately 14 percent below the in-air value just below the critical frequency. At the critical frequency, the wave speed appears to jump to values nearly equal to the unloaded values. Radiation patterns were obtained and when edge effects are eliminated, are in qualitative agreement with theoretical predictions for an infinite fluid-loaded plate.

TABLE OF CONTENTS

LIST OF FIGURES

LIST OF SYMBOLS

a Plate radius

c Flexural wave speed

c_o Sound velocity of the fluid

c_1 Plate wave velocity $[Eh/m(1-\sigma^2)]^{\frac{1}{2}}$

c_2 Shear wave velocity $[E/2\rho(1+\sigma)]^{\frac{1}{2}}$

c_3 Modified shear wave velocity $\frac{\pi}{\sqrt{12}}[eh/2m(1+\sigma)]^{\frac{1}{2}}$

D Plate bending stiffness $Eh^3/12(1-\sigma^2)$

E Young's modulus

F_o Driving force amplitude

h Plate thickness

i $(-1)^{\frac{1}{2}}$

k_o Acoustic wave number

m Mass of plate per unit area

P Acoustic pressure

(R,ϕ,θ) Spherical coordinates

ρ_o Density of the fluid medium

ρ Density of the plate material per unit volume

σ Poisson's ratio

α $(1-2\sigma)/2(1-\sigma)$

λ Flexural wavelength

ω Angular frequency

ω_c Critical (coincidence) frequency (Mindlin-Timoshenko)

ω_o Critical (coincidence) frequency (Classical)

ACKNOWLEDGEMENTS

The author would like to express his gratitude to Professor O. B. Wilson for his patience and for the guidance, experience, and motivation he provided throughout the preparation of this thesis. I would like to thank Mr. Robert Moeller for his assistance in fabricating the plates used in this work and commend him for his professionalism and the quality of his workmanship. Much appreciation is expressed to LCDR Tom Beeson and LCDR Rick Bostian for the assistance and moral support they provided. The financial support provided for this work by the Naval Torpedo Station, Keyport, Washington, is gratefully acknowledged.

I. INTRODUCTION

The purpose of this study was to provide some basic information which would support the problem of designing and developing a flexural-wave transducer suitable for the high frequency (75 kHz) acoustic ranging system used at the underwater weapons test ranges of the Naval Torpedo Station, Keyport, Washington. Previous work on the subject [Ref. 1] indicated the possibility of using a flexural-wave transducer as a broad-beam, broad-bandwidth sound source which would be readily adaptable to flush mounting, a necessary requirement for high speed torpedos. The possibility of using the torpedo hull itself as the radiating surface is especially attractive for low-drag, laminar flow shapes.

In the report of his experimental work on a flexural disk transducer, Sevdik [Ref. 1] discusses discrepancies between theoretical normal mode frequencies and measured values which were obtained for his transducers. He also discussed damping of the plate natural frequencies by fluid loading and inconsistencies in the change of phase speed with frequency for transducers of differing thickness.

Sevdik based his calculations on classical plate theory as described in Morse and Ingard [Ref. 2] and Malecki [Ref. 3]. Mindlin [Ref. 4] includes the effects of shear and rotatory inertia in a three-dimensional plate theory and states that classical plate theory begins to differ markedly from

three-dimensional theory at frequencies above that at which the flexural wavelength is about ten times the plate thickness. Mindlin's theory gives flexural-wave speed values for a given ratio of plate thickness to flexural wavelength which are lower than those from classical plate theory.

Alper and Magrab [Ref. 5] extend the Mindlin-Timoshenko plate theory to fluid-loaded plates and present calculated results showing decreasing plate natural frequencies resulting from fluid loading.

Feit [Ref. 6] considers the case of an infinite plate which is fluid loaded on one side and discusses significant changes in the theoretical radiation patterns that result at frequencies above and below the critical frequency, that frequency at which the flexural-wave speed in the plate equals the speed of sound in the fluid. Feit's work is also based on the Mindlin-Timoshenko theory.

The objective has been to determine experimentally the effects of fluid loading on the dispersion curves for flexural waves in a plate. The methods used included observation of the natural frequencies in a circular, free-edge plate in air and in water, and in some cases, measurements of the wavelengths of the flexural waves. The frequency range bracketed that for the critical wave speed.

A secondary object was to measure the radiation patterns for this circular plate. Some preliminary results are reported.

II. THEORETICAL CONSIDERATIONS

A. CLASSICAL PLATE THEORY

The classical differential equation of motion for the transverse displacement W of a plate is given by [Ref. 7, p. 1].

$$\nabla^4 W + \frac{m}{D}\frac{\partial^2 W}{\partial t^2} = 0 \tag{2.1}$$

Flexural wave speed is given by [Ref. 3, p. 508]

$$C = \left(\frac{D}{m}\right)^{1/4} \omega^{1/2} \tag{2.2}$$

Classical plate-vibration theory does not include the effects of rotary inertia, which were shown to reduce the natural frequencies of beams by Lord Rayleigh [Ref. 8], nor the effects of shear deformation, which were shown to be equally important by Timoshenko [Ref. 9]. The classical theory is valid for the case where the plate is thin compared to the flexural wavelength.

B. MINDLIN-TIMOSHENKO PLATE THEORY

Mindlin [Ref. 4] extended Timoshenko's theory for beams by including the effects of both shear and rotatory inertia in a three-dimensional plate theory. He has shown that the shear correction accounts almost entirely for the difference between classical plate theory and three-dimensional plate theory over the whole wavelength spectrum, and derived relationships for flexural wave speed as a function of the ratio plate thickness/flexural wavelength. For the case where only

the shear correction is considered [Ref. 4, p. 37]

$$\frac{C^2}{C_2^2} = \frac{2\pi^2}{3(1-\sigma)}\left(\frac{h}{\lambda}\right)^2\left[1 + \frac{2\pi^2}{3K^2(1-\sigma)}\left(\frac{h}{\lambda}\right)^2\right]^{-1} \tag{2.3}$$

where K is the root of

$$4\left[(1-\alpha K^2)(1-K^2)\right]^{1/2} = (2-K^2)^2, \quad 0 < K < 1 \tag{2.4}$$

Substituting for c_2 in equation 2.3 and rearranging gives

$$C^2 = \frac{\pi^2 E}{3\rho(1-\sigma^2)}\left(\frac{h}{\lambda}\right)^2\left[1 + \frac{2\pi^2}{3K^2(1-\sigma)}\left(\frac{h}{\lambda}\right)^2\right] \tag{2.5}$$

Letting

$$A = \frac{\pi^2 E}{3\rho(1-\sigma^2)} \tag{2.6}$$

And

$$B = \frac{2\pi^2}{3K^2(1-\sigma)} \tag{2.7}$$

Equation 2.5 reduces to

$$C^2 = A\left(\frac{h}{\lambda}\right)^2\left[1 + B\left(\frac{h}{\lambda}\right)^2\right] \tag{2.8}$$

Starting with the classical plate theory equation for flexural wave speed (2.2), substituting ρh for m, substituting for D, and squaring gives

$$C^2 = \omega\left[\frac{Eh^2}{12\rho(1-\sigma^2)}\right]^{1/2} \tag{2.9}$$

Substituting $\omega = \frac{2\pi C}{\lambda}$ and rearranging gives

$$C^2 = A\left(\frac{h}{\lambda}\right)^2 \tag{2.10}$$

Equations (2.8) and (2.10) relate flexural wave speed to for Mindlin's shear-corrected theory and classical plate theory, respectively. The constants A and B are determined by the properties of the plate material. For aluminum [Ref. 10]:

$\rho = 2700\ kg/m^3$

$E = 7.1 \times 10^{10}\ Nt/m^2$

$q = 0.33$

$K^2 = 0.8686$

$A = 9.71 \times 10^{10}(m/s)^2$

$B = 11.3$

Using these values, flexural-wave speed is plotted as a function of h/λ in Fig. 1. It can be seen that the shear-corrected value for flexural-wave speed begins to differ significantly from that given by classical plate theory for values of $\frac{h}{\lambda} > 0.10$. For Sevdik's 3 mm thick transducer at at 75 kHz, $\frac{h}{\lambda} \simeq 0.15$.

C. EFFECTS OF FLUID LOADING

Feit [Ref. 6] considers the case of an infinite, elastic plate, fluid-loaded on one side and excited by a time-harmonic point force. He derives an expression for the acoustic power radiated by this plate into an infinite half-space filled with an acoustic fluid. Because the velocity of sound in water is relatively high compared to the velocity of sound in air, the frequency at which the flexural wave speed in the plate exceeds the speed of sound in the fluid, i.e., the critical frequency, is relatively high. For this reason, Feit uses the Mindlin-Timoshenko plate theory in his work. Feit's equation for the farfield pressure is [Ref. 6, p. 1492]

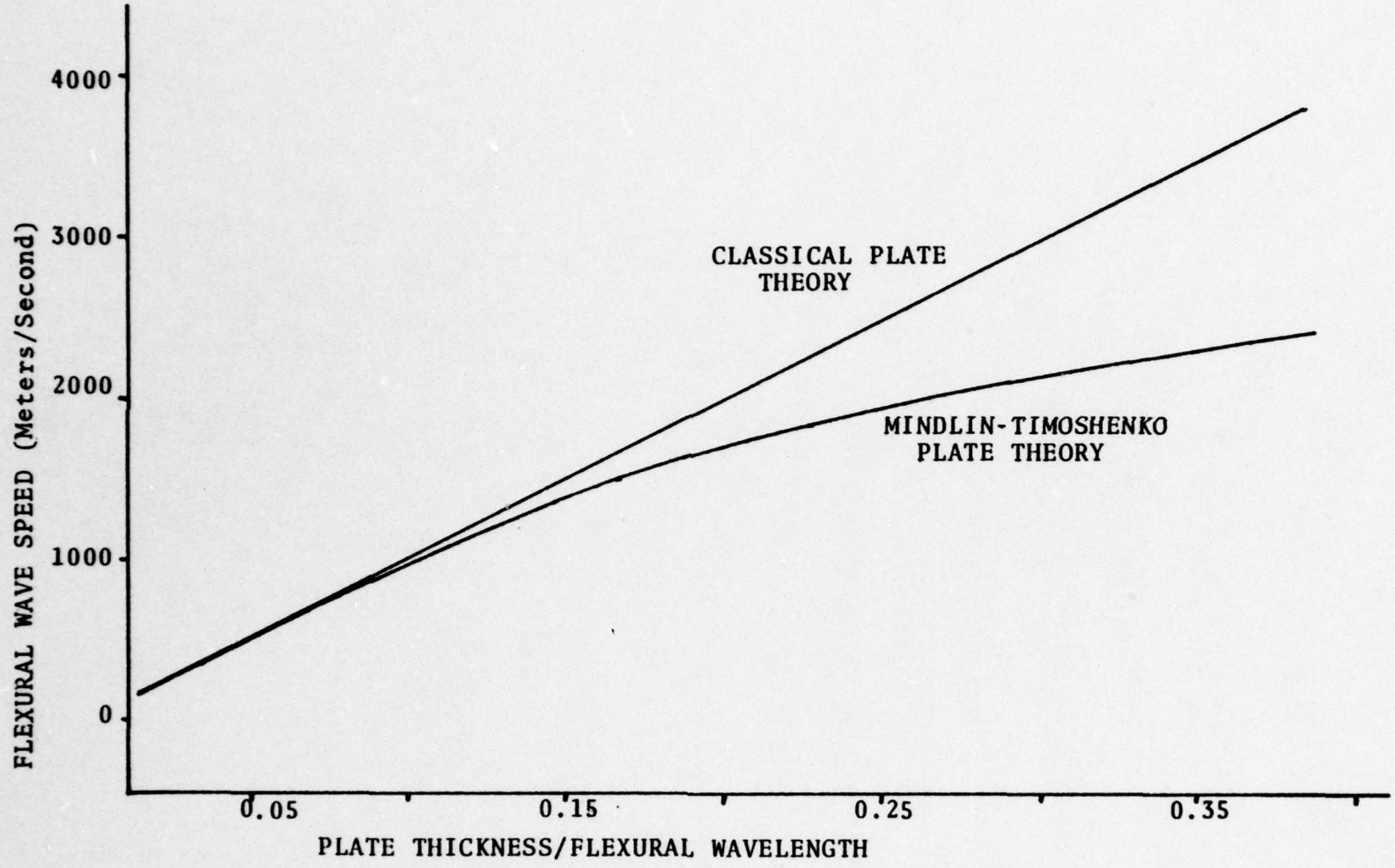

Figure 1. Comparison of Classical and Mindlin-Timoshenko Plate Theory

$$P(R,\phi,\theta) \simeq \frac{iF_0 k_0 e^{ik_0 R}}{2\pi R} \cos\phi \left[\frac{1+M}{1+M - \frac{i\omega m}{\rho_0 c_0} N \cos\phi} \right]$$

Where

$$M = \frac{\omega^2 h^2 c_1^2}{12 c_0^2 c_3^2} \left[\sin^2\phi - \frac{c_0^2}{c_1^2} \right]$$

And

$$N = \frac{\omega^2 h^2 c_1^2}{12 c_0^4} \left[\sin^2\phi - \frac{c_0^2}{c_1^2} \right] \left[\sin^2\phi - \frac{c_0^2}{c_3^2} \right]$$

(2.11)

and his expression for the critical frequency is

$$\omega_c = \omega_0 \left[\left(1 - \frac{c_0^2}{c_1^2} \right) \left(1 - \frac{c_0^2}{c_3^2} \right) \right]^{-1/2} \qquad (2.12)$$

Feit's theory predicts significant changes in the radiation patterns from the infinite plate at frequencies above and below the critical frequency. Quoting Feit [Ref. 6, p. 1493],

> Below coincidence, the propagating flexural wave does not radiate energy away from the plate. Therefore, the radiated sound pressure can be associated with the non-propagating nearfield deflection of the plate, which acts like a small piston and therefore is relatively non-directive.
>
> Above coincidence, the situation is quite different. In this range, the phase speed of the propagating flexural wave exceeds that of the sound wave, and therefore the propagating wave can itself radiate energy away from the plate in a definite direction.

Alper and Magrab [Ref. 5] extend the Mindlin-Timoshenko plate theory to the case of clamped-edge circular plates with fluid loading on one side. They present results based on computations using their theory for the case of a thin

(thickness/radius = 0.04) and a thick (thickness/radius = 0.2) steel plate in sea water. Their results indicate a significant reduction in the plate natural frequencies when fluid loaded which is more pronounced for the thin plate. They also conclude that for the same driving force the thin plate will radiate considerably more power into the water and that the thin plate produces a more directional radiation pattern for a given driving frequency.

III. EXPERIMENTAL PROCEDURE

A. FLEXURAL WAVE SPEED MEASUREMENTS

Several experimental techniques were used to measure flexural wave speed as a function of frequency.

Initial measurements were made with a 1/4 in. thick rectangular steel plate, 64.5 cm by 76.5 cm. The plate was driven by a longitudinal vibrator composed of four 1/4 in. thick, 3/4 in. diameter piezoceramic elements. Brass masses 1/4 in. thick and 3/4 in. in diameter were added at each end of the ceramic elements and the unit was clamped together with a screw threaded into the bottom disk. The unmounted driver was resonant at 34.01 kHz. The driver was mounted near the geometric center of the plate with epoxy cement. With the driver mounted on the plate, over 105 resonances were detected between 10 kHz and 40 kHz using measurements of the electrical admittance of the driver transducer.

Two different experimental techniques were employed in measuring flexural wave speed. The first procedure was to use a small accelerometer to measure the phase and amplitude of the wave in the plate along a radial line from the driver transducer while the plate was excited continuously at one frequency. The equipment used in this procedure is listed below and connected as shown in Fig. 2.

Hewlett Packard 3590A/3594A Wave Analyzer/Oscillator
Dranetz Model 305 Digital Phase Meter
Tektronix 547 Dual Trace Oscilloscope
Hewlett Packard 465A Voltage Amplifier
Hewlett Packard 467A Power Amplifier
Data Precision 5740 Frequency Counter

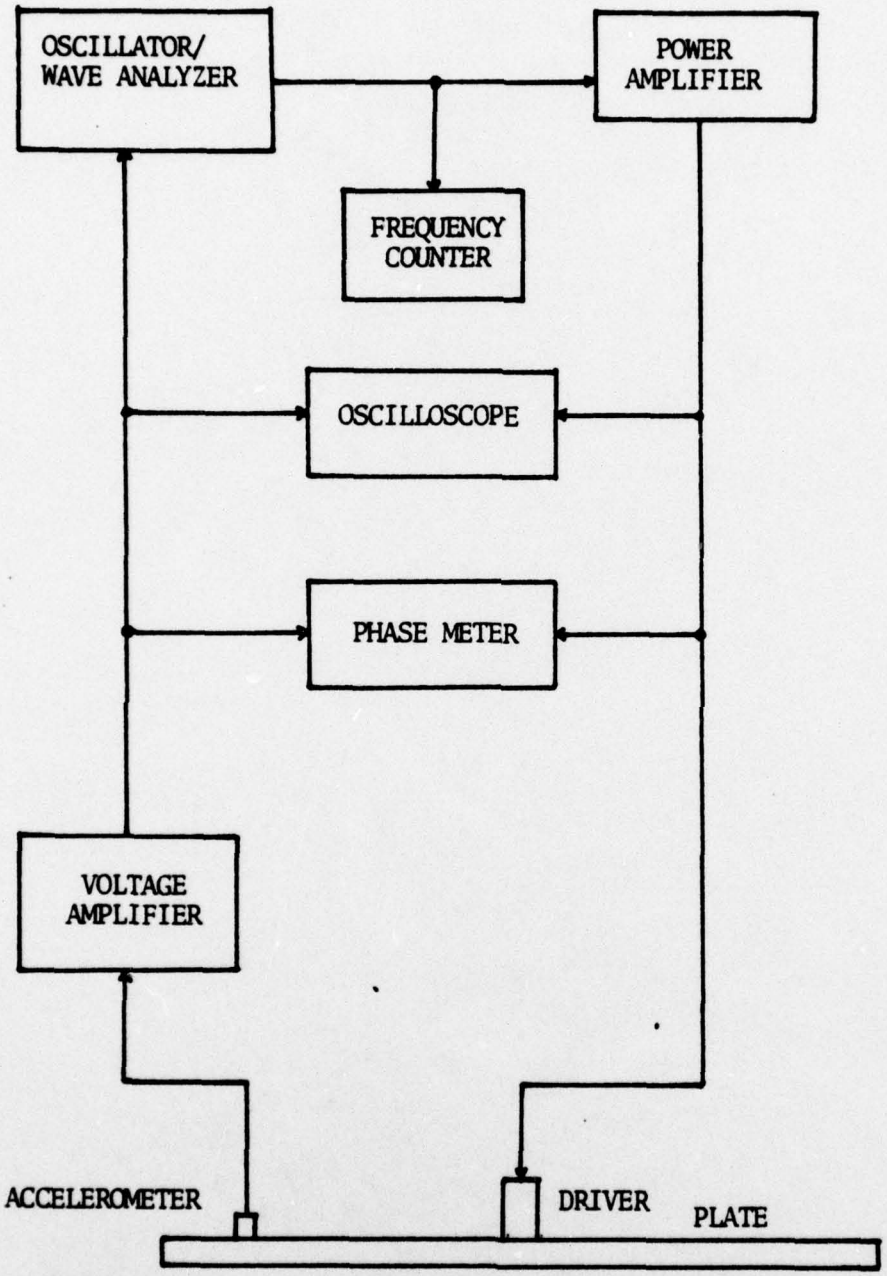

Figure 2. Phase/Amplitude Measurement Apparatus

Using the driving voltage as the reference for the phase-meter and the voltage generated by the accelerometer to measure the phase of the motion of the plate, measurements were made at one-half cm intervals over a distance of 15 cm. From the measured values of total phase change over the known distance, flexural wavelength could be determined.

Two difficulties were encountered using this technique. First, acquiring data was a slow and time-consuming process. A thin layer of grease was smeared along the line over which the measurements were made to get good contact between the accelerometer and the plate. It was found that the values of phase and amplitude obtained would vary depending upon how the accelerometer was placed on the plate. To compensate for this variation and positioning error, a minimum of three sets of measurements were made at each frequency. This required a minimum of 90 measurements to obtain one value of flexural wavelength versus frequency. Secondly, it was found that because of the very complicated modal structure in the plate due to asymmetry, the phase data did not give reliable wavelength values. Due to these difficulties, this technique was abandoned.

The second technique used was to excite the plate with a short (four cycle) pulse. By measuring the travel time of a specific cycle of the pulse over a known distance, flexural wave speed could be determined. This method also eliminated the complex standing wave patterns resulting from continuous excitation. The test equipment used for these measurements

is listed below and depicted schematically in Fig. 3.

Hewlett Packard 3590A/3594A Wave Analyzer/Oscillator
Data Precision 5740 Frequency Counter
General Radio 1398A Tone Burst Generator
Tektronix 547 Dual Trace Oscilloscope
Hewlett Packard 465A Voltage Amplifier
Hewlett Packard 467A Power Amplifier
40 dB Gate/Harrison 6205B DC Power Supply

The driving voltage was used as a reference and wave travel time measurements were made using the delayed sweep feature of the oscilloscope. Six measurements were made at each frequency and averaged to compensate for error in positioning the accelerometer. These data are plotted in Fig. 4 in comparison with a curve obtained from Mindlin (Eqn. 2.8). Error bars, the average deviation above and below the mean of the six values, are plotted to indicate typical variability of the data.

The next procedure was to measure the flexural-wave speed with one surface of the plate in contact with water. A three-inch high plywood dam, two feet on a side, was secured and sealed to the plate which permitted making measurements on the top of the plate with the accelerometer while the plate essentially floated horizontally in the anechoic tank. The pulse method was used to measure wave speed and six measurements were made and averaged, as was done with the in-air data. These data are also plotted with the in-air data in Fig. 4. As can be seen, the in-water data do not differ significantly from the in-air data. The reason for this result is not certain since it was expected that the flexural-wave speed values would be lower for a given frequency in water.

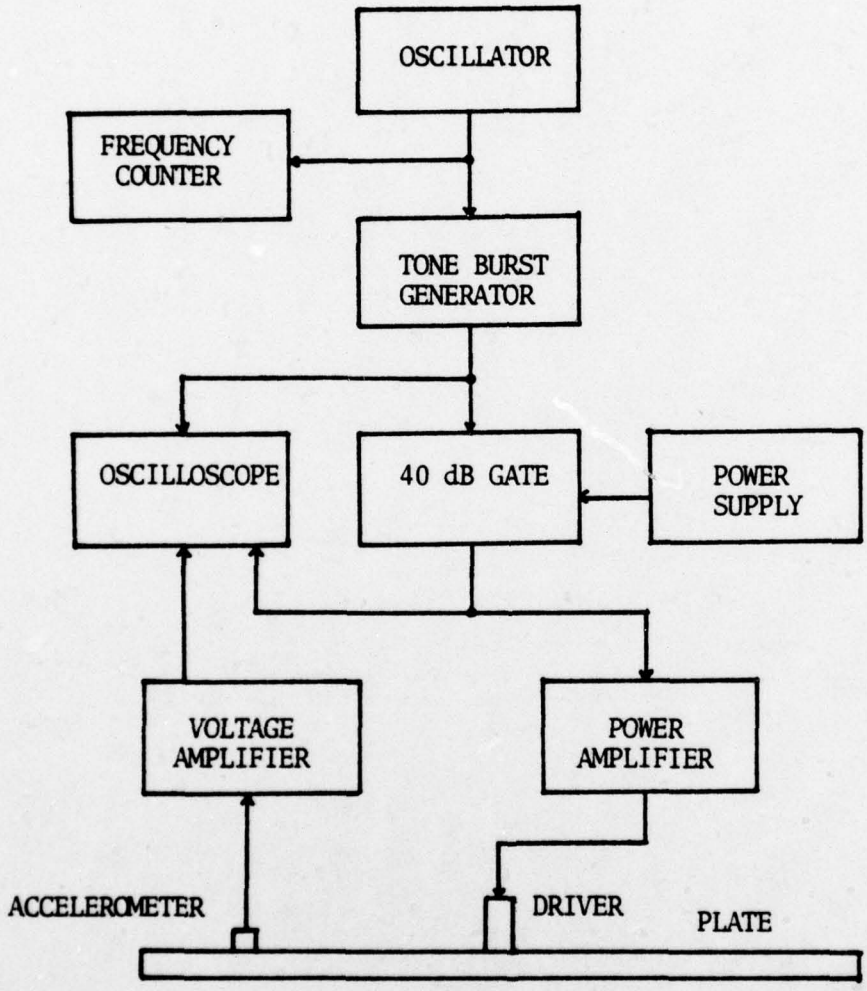

Figure 3. Pulse Measurement Apparatus

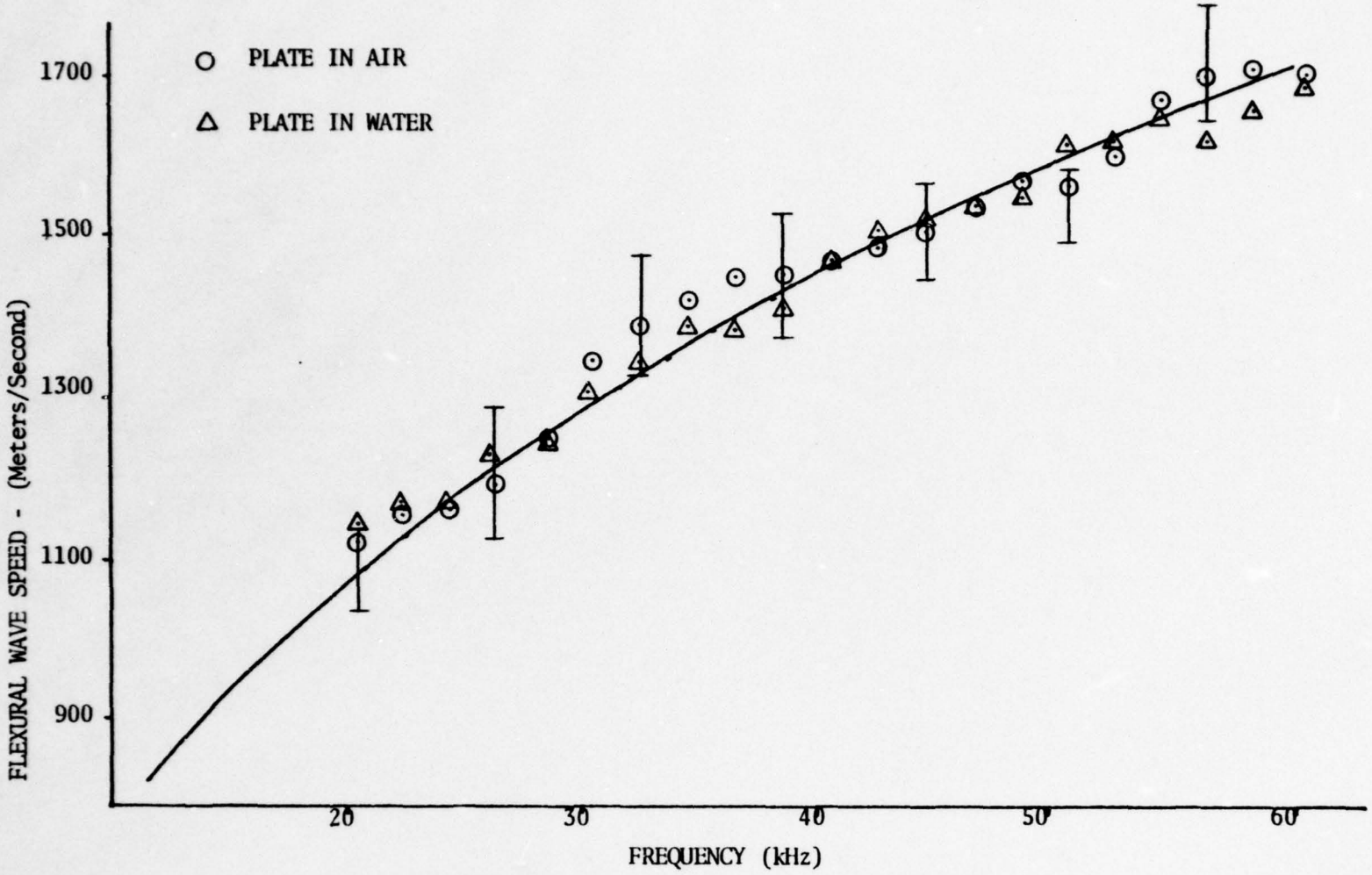

Figure 4. Steel Plate Flexural Wave Speed

Work with the steel plate was discontinued at this point due to the complexity of the modal structure and the difficulty in handling the large weight.

Measurementswere continued on a round aluminum plate, 25 in. in diameter and 5/16 in. thick. It was driven at the center by the same stack of ceramic elements and a three-inch high sheet aluminum dam was secured and sealed to the perimeter of the plate to permit making measurements with one side of the plate in contact with water. The plate with dam was buoyant and floated approximately one inch deep in the anechoic tank. Using the pulse method, six sets of data were obtained in air and in water. These data were even more irregular and scattered than the data obtained with the steel plate. However, it was observed that dispersion effects in the propagation of the wave pulse contributed significantly to the problem of measurement of the phase speed. These effects may also have been a contributor to the problems with measurements on the steel plate described above. Because of the difficulties encountered using the pulse method to obtain data, it was discontinued.

B. PLATE RESONANCE FREQUENCY MEASUREMENTS

Another approach to the observation of the effects of fluid loading on the flexural waves in the plate was used. This was accomplished by measuring the frequencies of the flexural-wave normal modes for the free-edge circular plate. The electrical admittance of the driving transducer provides one method for observing the plate resonances. The equipment listed below

was connected as shown in Fig. 5 for this procedure:

Hewlett Packard 3590A/3594A Wave Analyzer/Oscillator
Hewlett Packard 7035B X-Y Plotter
Hewlett Packard 465A Voltage Amplifier
Hewlett Packard 467A Power Amplifier
Dranetz 100C Complex Impedance/Admittance Meter
Data Precision 5740 Frequency Counter

As can be seen from the equipment diagram, the wave analyzer was used to drive the X axis of the plotter. Plots of conductance versus frequency were made rather than plots of conductance and susceptance because they presented a more graphic picture of the normal mode frequencies. Fig. 6 is representative of the plots obtained using this technique. In an attempt to identify each mode, theoretical values were calculated using eigenvalues obtained from Leissa [Ref. 7, p. 11]. Because Leissa's values are computed from classical plate theory and because of the effect of the mass loading of the driver on the plate, the theoretical frequencies could not be directly correlated with the experimental values. Therefore, an experimental procedure was needed to determine which mode was excited at a given frequency. This was carried out by mapping the modal structure in the plate using an accelerometer. It was found in making measurements at those frequencies where peaks occurred in the conductance vs. frequency plots that only modes with nodal circles were detected. The amplitude of the signal generated by the accelerometer remained constant when the accelerometer was moved in a circle about the center of the plate. It was also found that the nodal circles (amplitude minimums) were quite regularly spaced for the higher order modes ($n > 8$). By measuring the spacing

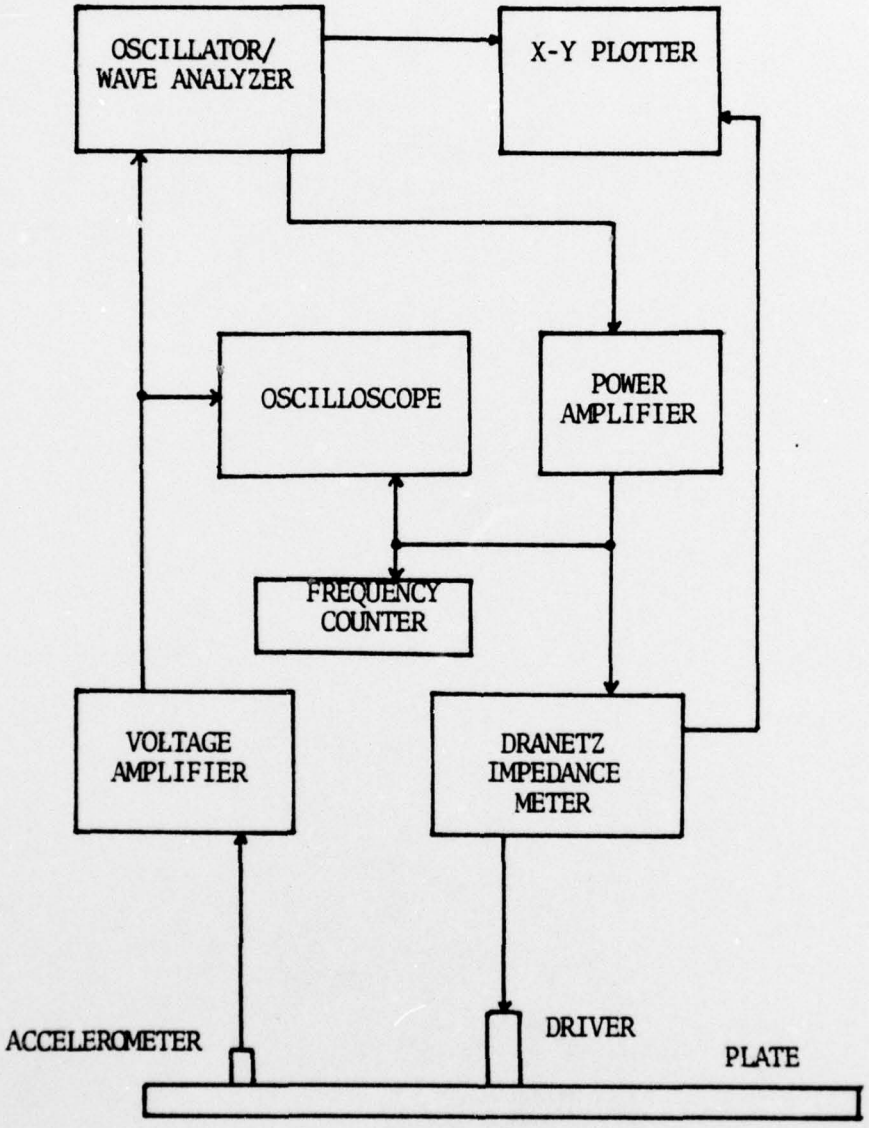

Figure 5. Nodal Circle Measurement Apparatus

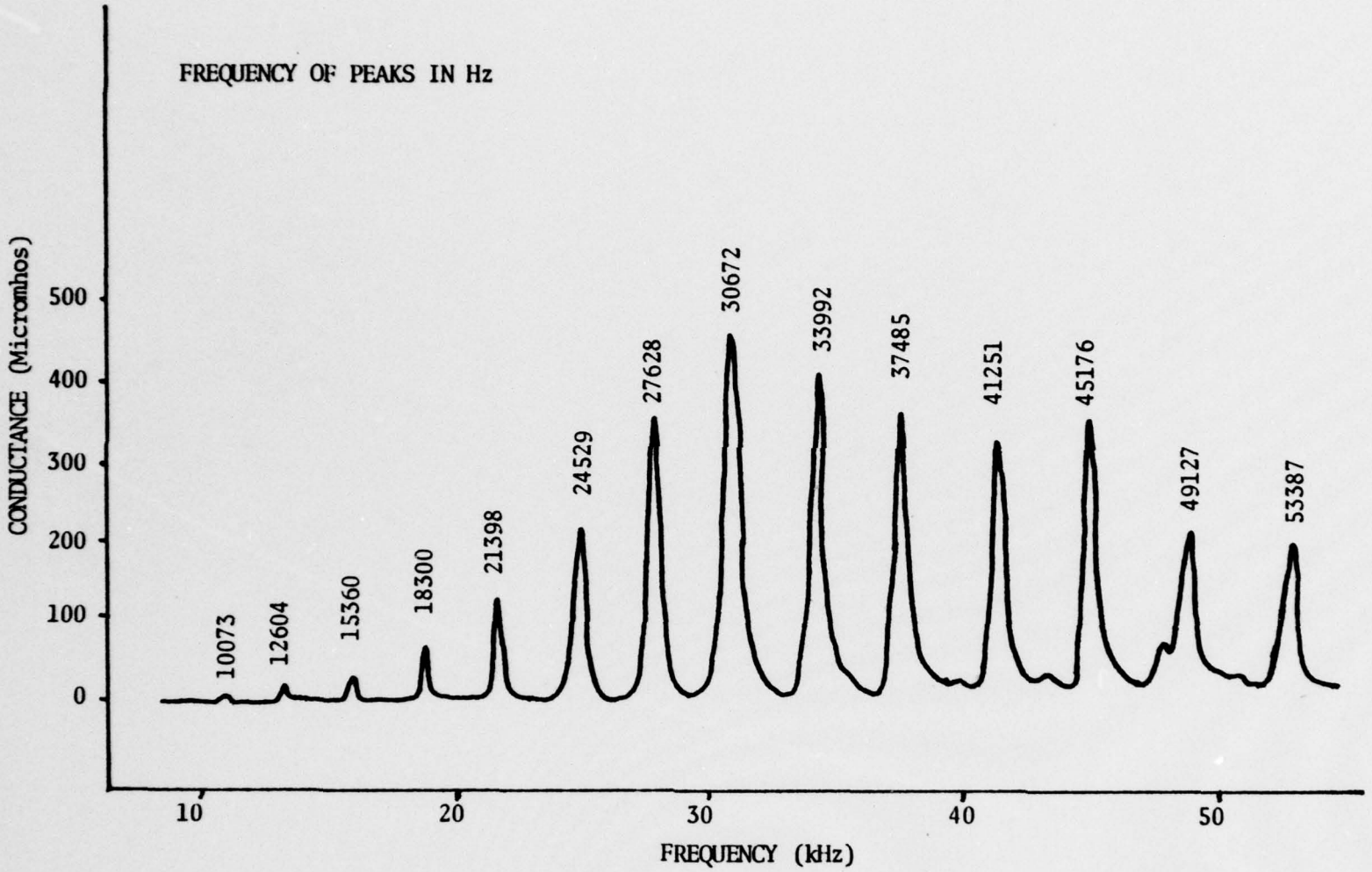

Figure 6. Conductance/Frequency Plot, Aluminum Plate in Air

between nodal circles at the plate natural frequencies detected with the Dranetz meter, flexural wavelength could be measured quite accurately as a function of frequency. The assumption that the spacing between two nodal circles is equal to one-half flexural wavelength is justified in Appendix A.

The initial nodal circle measurements were made with the sheet aluminum dam removed to more closely approach a free edge boundary condition. To permit making measurements in water, a dam was made from 0.011 in. thick natural rubber sheet. The rubber sheet was stretched across the bottom of the plate and secured to the sheet metal ring used previously, with about one inch of free rubber between the plate and the supporting ring. The plate was suspended using heavy nylon cord fastened at eight regularly spaced points around the top of the aluminum ring. To ensure the plate was loaded by the water, the thin space between the bottom of the plate and the rubber sheet was filled with transducer oil having a specific acoustic impedance equal to that of water and all air bubbles carefully removed. This arrangement is depicted in Fig. 7. The stack of four ceramic elements used in the previous experiments was used to excite the plate. Fig. 8 is the conductance vs. frequency plot for the plate suspended in the rubber dam in air. The flexural wavelength data obtained using the nodal-circle method is summarized in Table I and plotted in Fig. 9. Figures 10 and 11 present the conductance vs. frequency plots obtained with the plate in water. The in-water data are summarized in Table II and are plotted with

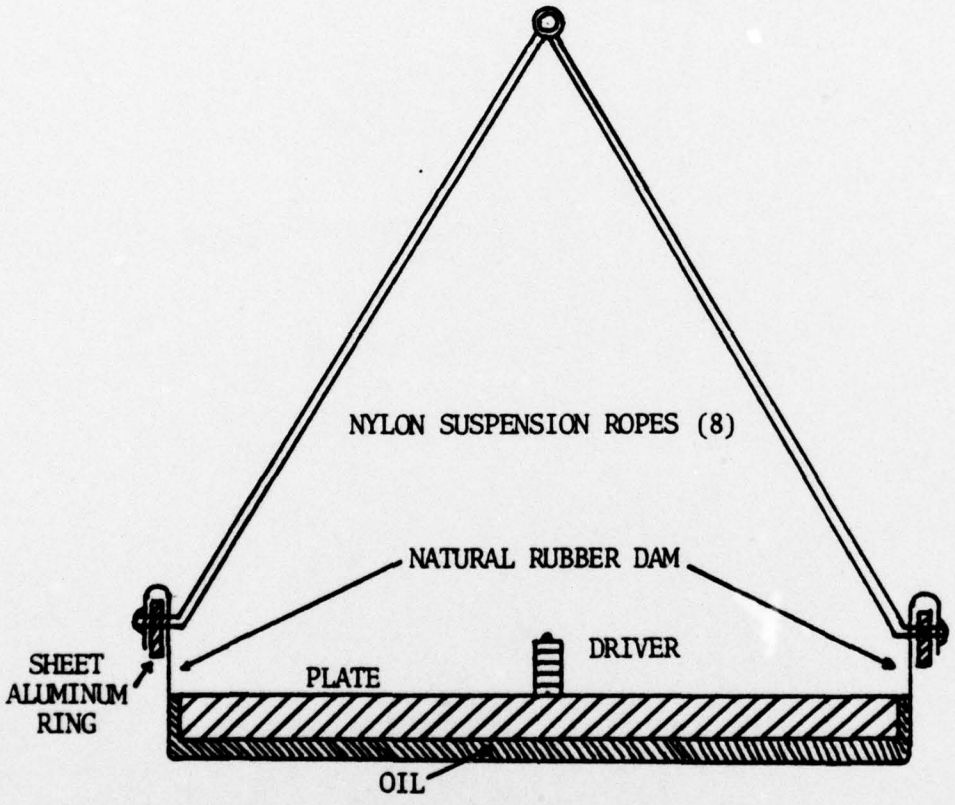

Figure 7. Plate Suspension Apparatus (not to scale)

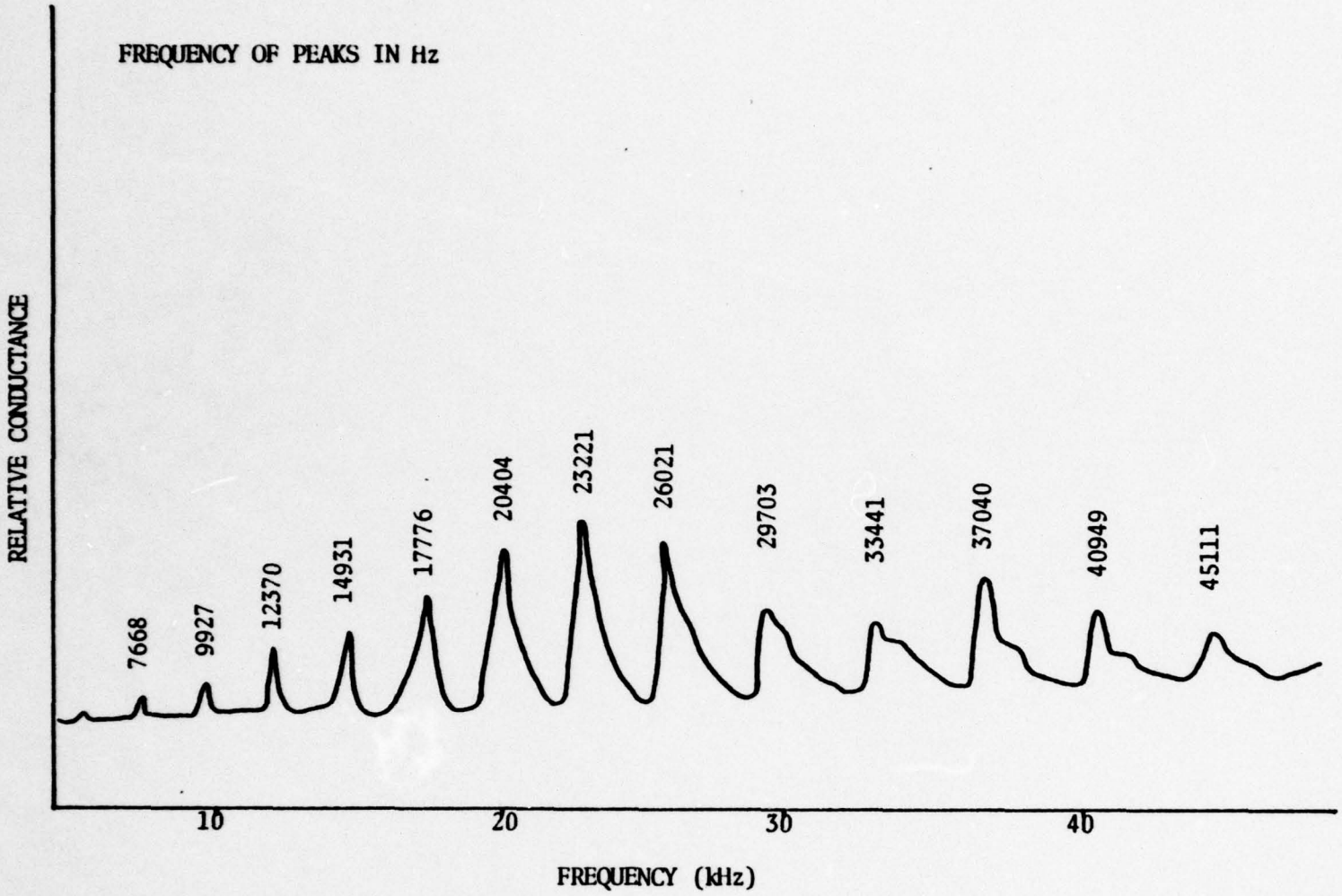

Figure 8. Conductance/Frequency Plot, Plate in Air in Rubber Dam.

TABLE I

NODAL CIRCLE DATA IN AIR

Frequency	Radial Distance	Number of Wavelengths	Flexural Wavelength	Flexural Wave Speed
7764 kHz	18.8 cm	2	9.40 cm	730 m/s
10048	25.5	3	8.50	854
12586	21.8	3	7.30	919
15366	27.5	4	6.90	1060
18274	24.4	4	6.10	1115
21229	22.4	4	5.60	1189
24085	26.0	5	5.20	1252
29695	28.2	6	4.70	1396
33216	31.5	7	4.50	1495
36794	24.8	6	4.13	1520
39983	23.2	6	3.87	1547
46749	25.2	7	3.60	1683
51236	23.9	7	3.41	1749

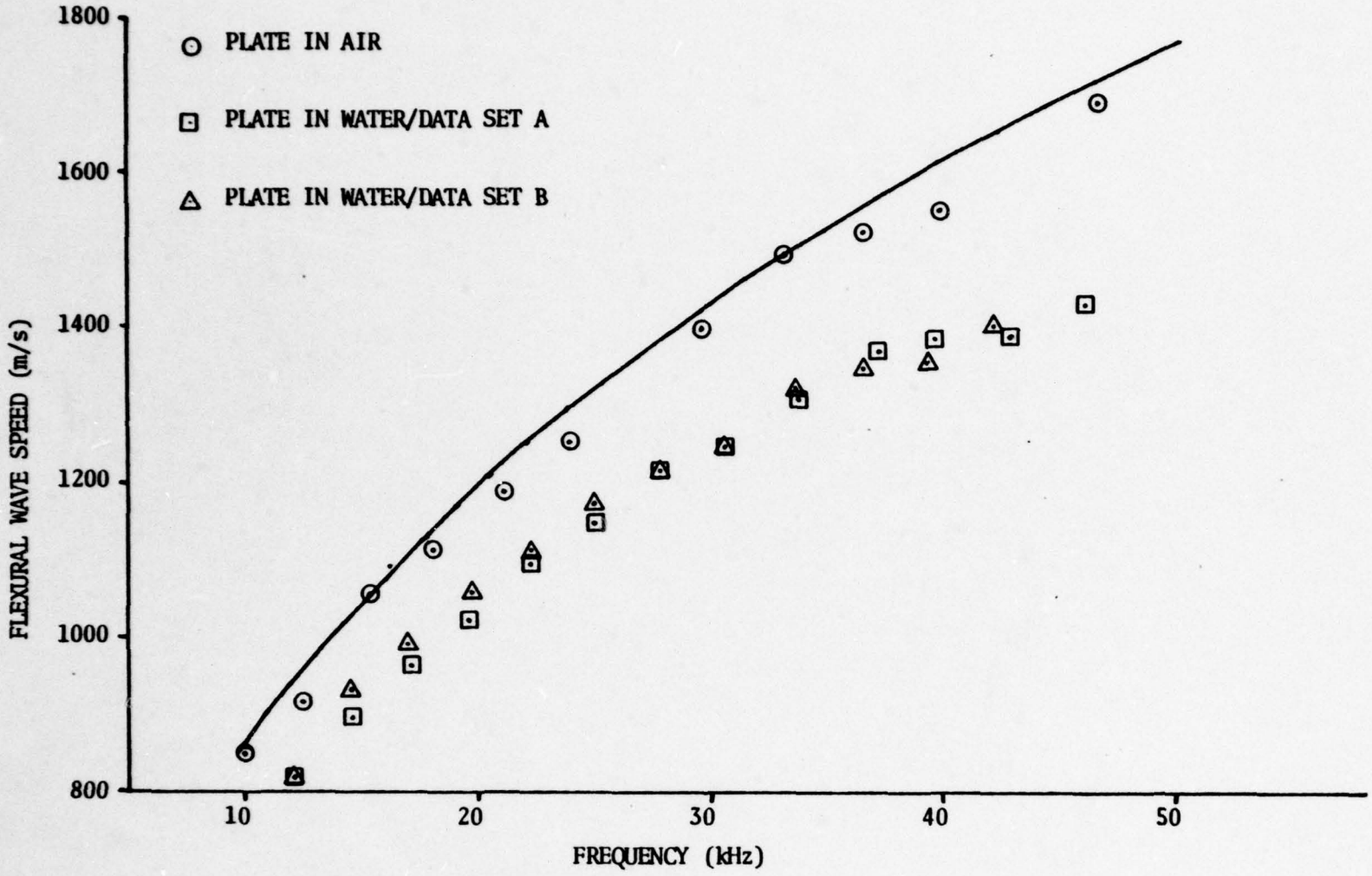

Figure 9. Aluminum Plate Flexural Wave Speed

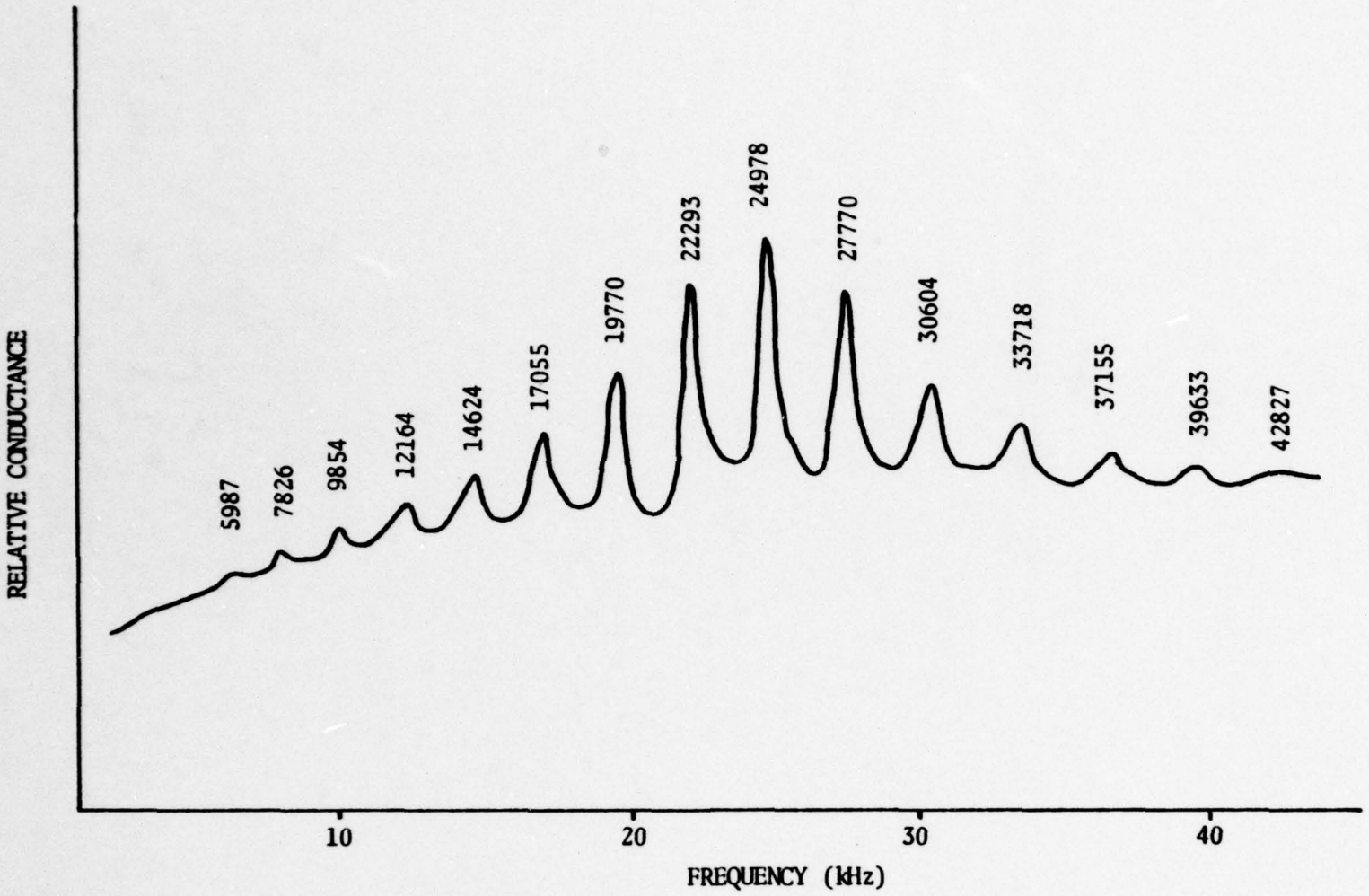

Figure 10. Conductance/Frequency Plot, Plate Suspended in Water.

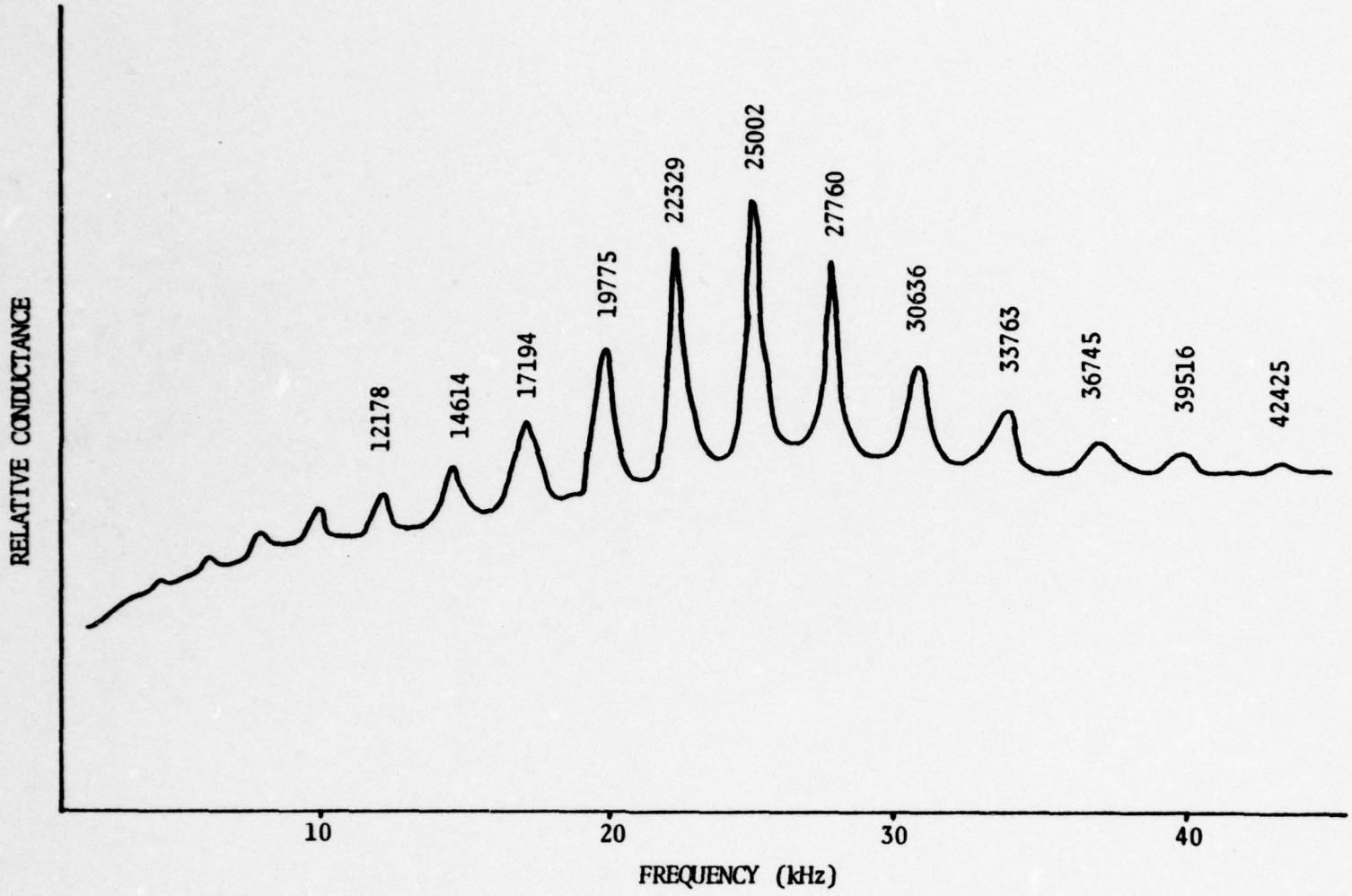

Figure 11. Conductance/Frequency Plot, Plate Suspended in Water

TABLE II

NODAL CIRCLE DATA IN WATER

Frequency	Radial Distance	Number of Wavelengths	Flexural Wavelength	Flexural Wave Speed
12164 Hz	27.2 cm	4	6.80 cm	827 m/s
14624	27.7	4.5	6.16	900
17055	28.4	5	5.68	969
19770	28.4	5.5	5.16	1021
22293	29.6	6	4.93	1100
24978	27.6	6	4.60	1149
27770	26.2	6	4.37	1213
30604	24.4	6	4.07	1245
33718	23.3	6	3.88	1309
37155	22.0	6	3.67	1362
39633	20.9	6	3.48	1381
42827	19.4	6	3.23	1385
46002	18.6	6	3.10	1426
SET 2				
12178	20.4	3	6.80	828
14614	25.5	4	6.38	932
17194	23.2	4	5.80	997
19775	26.8	5	5.36	1060
22329	25.0	5	5.00	1116
25002	23.5	5	4.70	1175
27760	26.2	6	4.37	1213
30636	24.4	6	4.07	1247
33673	23.6	6	3.93	1323
36745	22.0	6	3.67	1349
39516	20.6	6	3.43	1355
42425	19.8	6	3.30	1400

the in-air data in Fig. 9. As can be seen, the in-air data are in good agreement with the Mindlin theory and the flexural wave speed with water loading is significantly lower than it is in air. The highest wave speed values obtained in water were just above 1400 m/s, which is below the sound speed in water. Since it was desired to investigate the flexural-wave speed in water at frequencies where it exceeded the sound speed in water, a new driver was fabricated from two 3/8 in. diameter, 1/4 in. thick piezoceramic elements. With this driver mounted on the plate, in-air nodal-circle data were obtained to above 80 kHz. These data are summarized in Table III and plotted with the data obtained previously in Fig. 13. Fig. 12 is the conductance vs. frequency plot with the plate suspended in air using the small driver, and Fig. 14 is the corresponding plot with the plate in water. It exhibits none of the structure of the previous plots and in-water data could not be obtained using the nodal-circle technique.

Because the plate natural frequencies could not be detected using the small driver with the plate in water, a second technique was used to extend the in-water measurements to 80 kHz. Using an oscilloscope with vertical and horizontal sweeps, Lissajous patterns were used to measure the rate of change of the phase difference between the driving voltage and the voltage generated by the accelerometer as a function of the distance from the driving transducer. These data are summarized in Table IV. As can be seen, the data obtained by this technique differ from the data obtained using the nodal

TABLE III

IN-AIR DATA/NODAL CIRCLE TECHNIQUE WITH SMALL DRIVER

Frequency	Radial Distance	Number of Wavelengths	Flexural Wavelength	Flexural Wave Speed
45643 Hz	21.8 cm	6	3.63 cm	1658 m/s
49832	20.8	6	3.47	1728
54089	19.7	6	3.28	1776
58466	19.4	6	3.23	1890
62870	18.0	6	3.00	1886
67381	17.1	6	2.85	1920
71991	16.9	6	2.82	2027
76560	15.7	6	2.62	2003
80976	15.3	6	2.55	2060

TABLE IV

IN-WATER DATA/SMALL DRIVER/LISSAJOUS PATTERN TECHNIQUE

Frequency	Radial Distance	Number of Wavelengths	Flexural Wavelength	Flexural Wave Speed
40000 Hz	21.0 cm	6	3.50 cm	1400 m/s
45000	18.2	5	3.64	1638
45760	18.6	6	3.10	1418
50000	13.8	4	3.45	1725
55000	16.0	5	3.20	1760
60000	15.5	5	3.10	1860
65000	18.2	6	3.03	1971
74887	13.2	5	2.64	1977

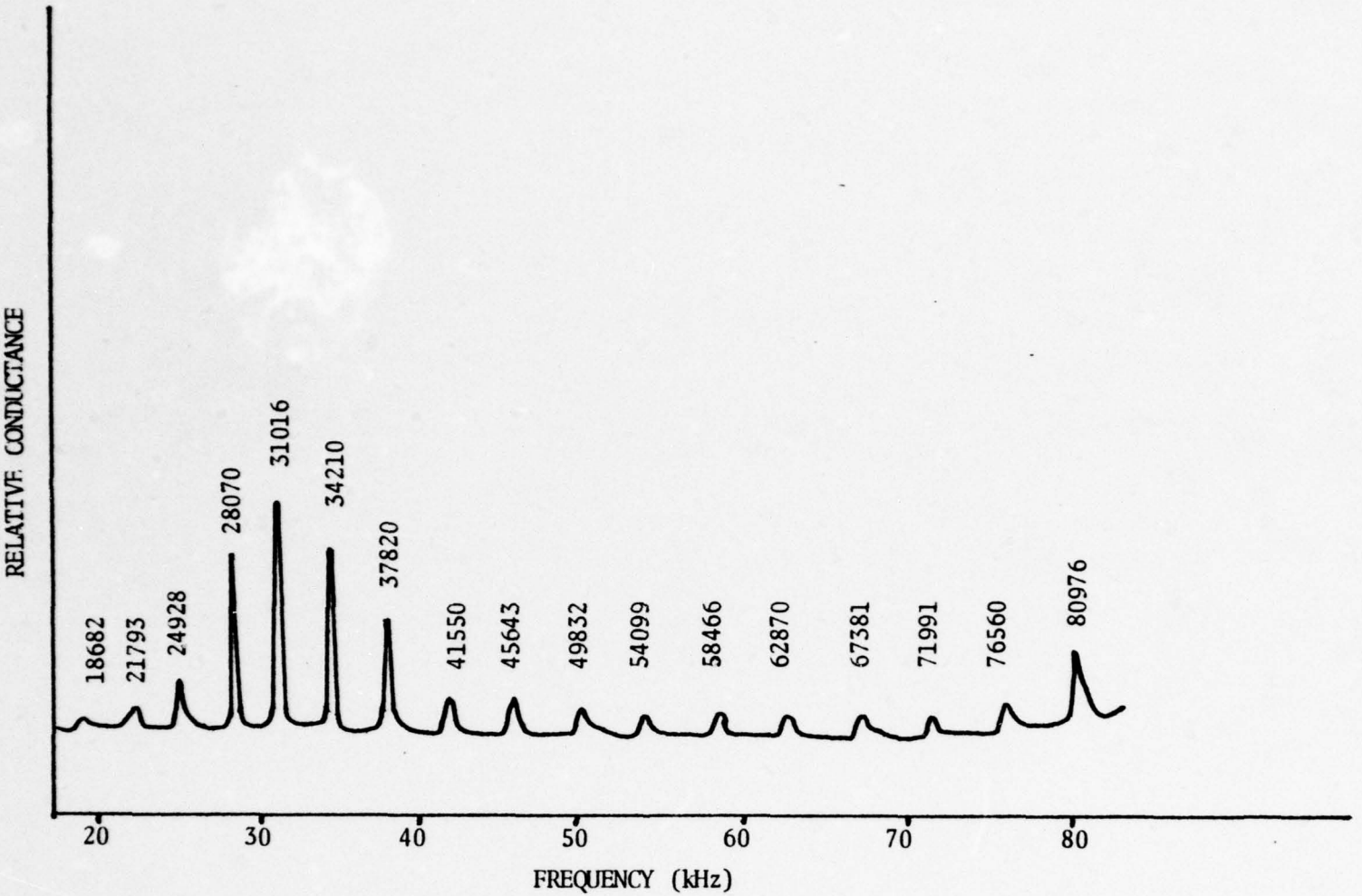

Figure 12. Conductance/Frequency Plot, Small Driver, Plate in Air

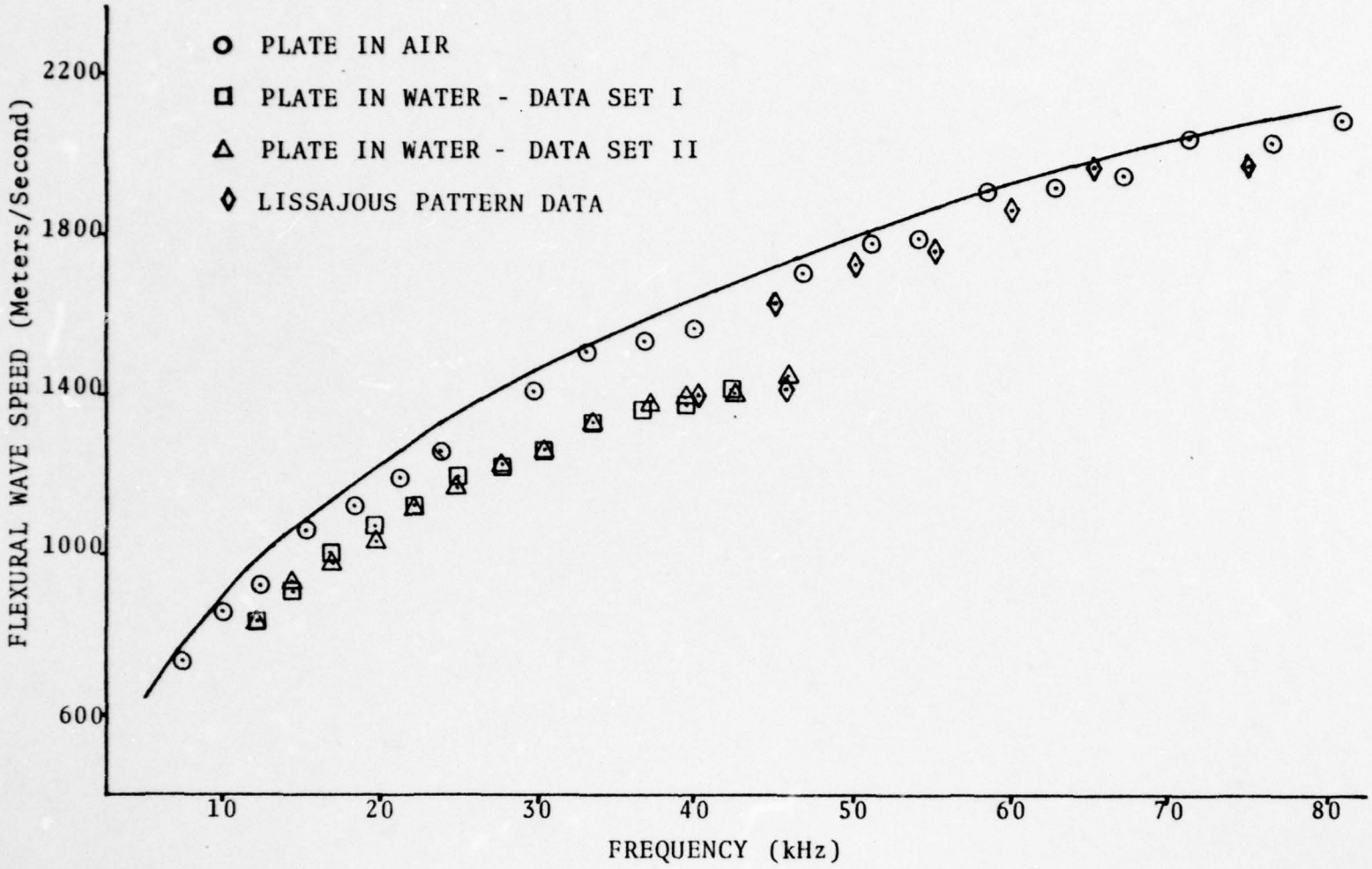

Figure 13. Aluminum Plate Flexural Wave Speed

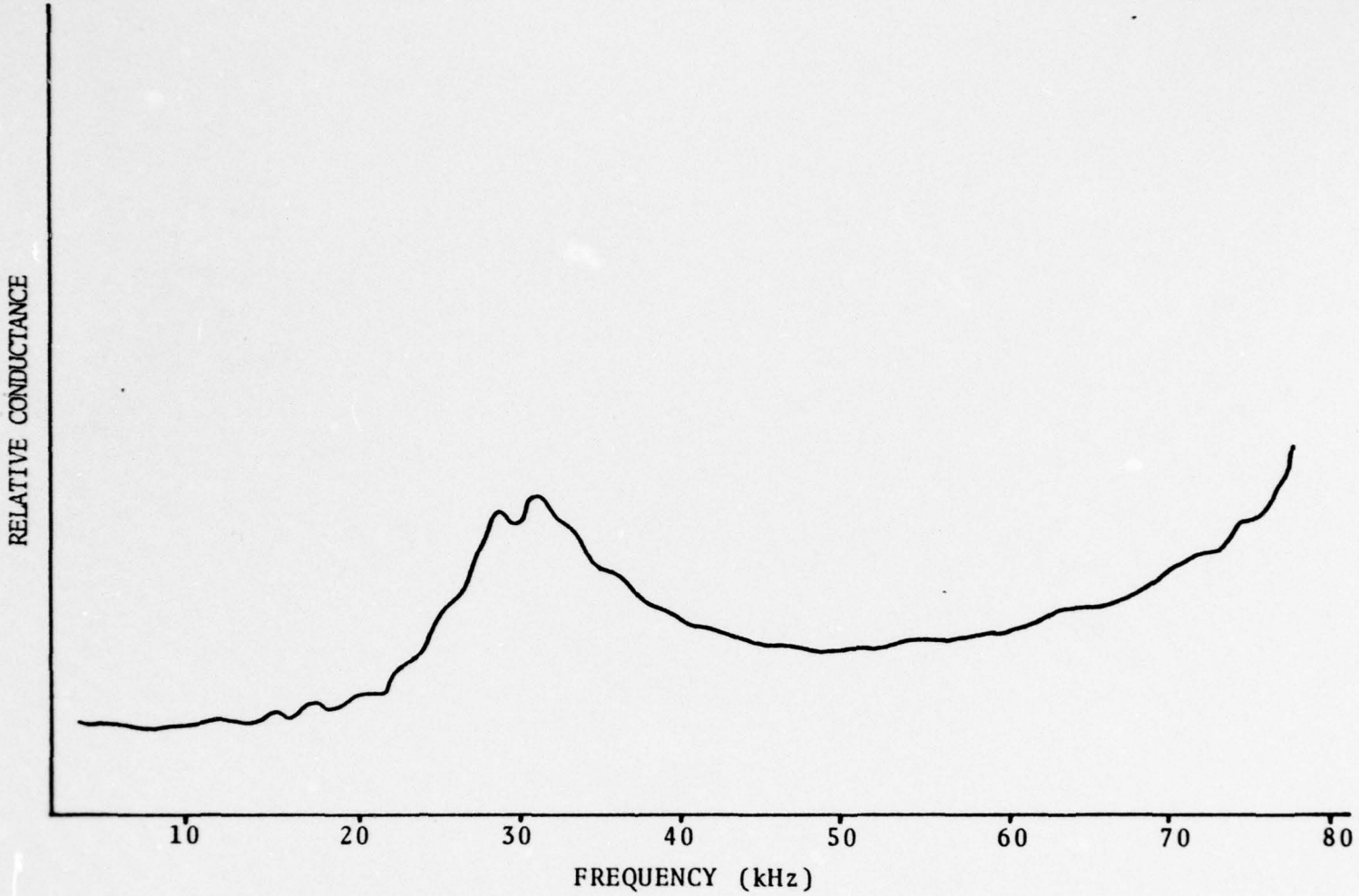

Figure 14. Conductance/Frequency Plot, Small Driver, Plate in Water

circle technique. The reasons for this observed difference in flexural-wave speed values may involve the differing measurement techniques. In order to compare the techniques, six measurements were made in air using each method between 28 kHz and 50 kHz over a distance of five wavelengths. The values obtained by the two methods agree within five percent whereas the observed change in flexural wave speed was 15 percent. The effect of radiation impedance is clearly changing since the normal modes are highly damped above the critical frequency, so the observed changes in flexural wave speed may be real.

C. RADIATION PATTERN MEASUREMENTS

Alper and Mabrab [Ref. 5] present theoretical radiation patterns for two cases of steel plates with clamped edges. The radiation patterns are computed for frequencies only up to the fifth in-fluid resonant frequency which corresponds to approximately four kHz for the circular aluminum plate used in this work.

Feit [Ref. 6] presents theoretical results for an infinite plate which is fluid loaded on one side. Based on the Mindlin-Timoshenko theory, he predicts significant differences in the radiation patterns for the infinite plate at frequencies above and below the critical frequency. Below the critical frequency the theoretical beam patterns are nearly omnidirectional, whereas above the critical frequency theory predicts the radiation pattern to be composed of two major side lobes. For a frequency equal to 1.5 times the critical frequency,

Feit's theory predicts these lobes to be approximately 60 degrees off the plate axis. For a steel plate, Feit's theory predicts that the critical frequency based on the Mindlin-Timoshenko theory is approximately 23 percent higher than predicted by classical plate theory.

A series of radiation patterns was made with the circular aluminum plate in order to compare theory with experiment. The radiation patterns were made in one of the anechoic water tanks at the Naval Postgraduate School.

In order to limit acoustic loading to one side of the plate, the back of the plate was covered with a sheet of 1/4 in. thick neoprene foam, the same type of material used for a skin diver's wet suit. The driver transducer was enclosed in a plastic cup sealed to the neoprene, which provided electrical and mechanical isolation from the water. The neoprene layer was glued on at the edge of the plate.

The below listed equipment was used to make the radiation pattern measurements and is depicted schematically in Fig. 15.

Hewlett Packard 7035B X-Y Plotter
Tektronix RM 561A Dual Trace Oscilloscope
Hewlett Packard 3594A Sweeping Oscillator
General Radio 1396A Tone Burst Generator
40 dB Gate
Harrison 6205B DC Power Supply
Hewlett Packard 465A Power Amplifier (2)
Krohn-Hite DCA 50R 50-Watt Power Supply
Hewlett Packard 465A Voltage Amplifier
Arenberg Ultrasonic Laboratory Attenuator
Envelope Detector
PAR Model 160 Boxcar Integrator
Hewlett Packard/Moseley 7561A Logarithmic Converter
Data Precision 5740 Frequency Counter
Hewlett Packard 400E AC Voltmeter
LC-10 Hydrophone

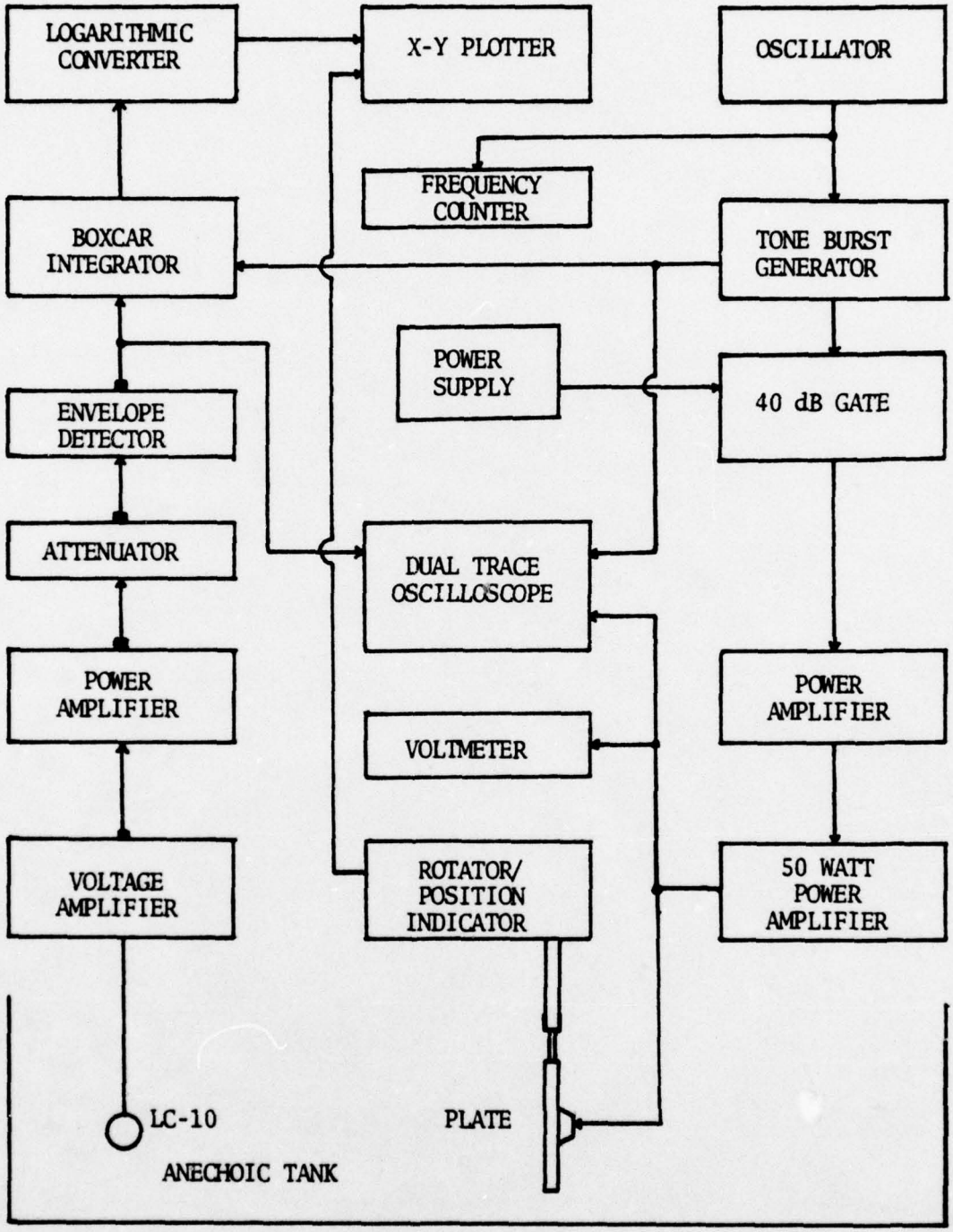

Figure 15. Radiation Pattern Measurement Apparatus

The mechanical drive used to rotate the plate includes a potentiometer on the gear train which produces a DC voltage proportional to the angular position of the plate. This voltage was applied to the X axis of the X-Y plotter. The calibrated LC-10 hydrophone used as a receiver and the plate were separated by a distance of 5 meters with the hydrophone and the center of the plate at a depth of 1.92 meters.

The output of the hydrophone was amplified, rectified by the envelope detector and then fed to the boxcar integrator. By using a pulsed signal and gating the integrator to integrate only over the direct path signal, interference effects from the air surface reflected signal are eliminated. The integrator produces a DC voltage which is proportional to the average amplitude of the received pulse envelope. Using the logarithmic converter permits the plotting of a large dynamic range of received signal.

The attenuator shown in Fig. 15 was used to calibrate the Y axis of the radiation pattern plots. This was necessary because of the non-linearity of the envelope detector. Each radiation pattern was calibrated by varying the drive voltage to obtain a full scale reading on the integrator (10 V. DC output from the integrator) and then incrementing the attenuation in 3 dB intervals. The drive voltage was then reset to 80 V. RMS prior to generating the radiation pattern. The radiation patterns are shown in Figs. 16 through 31, and Table V is a summary of the equipment settings for each pattern.

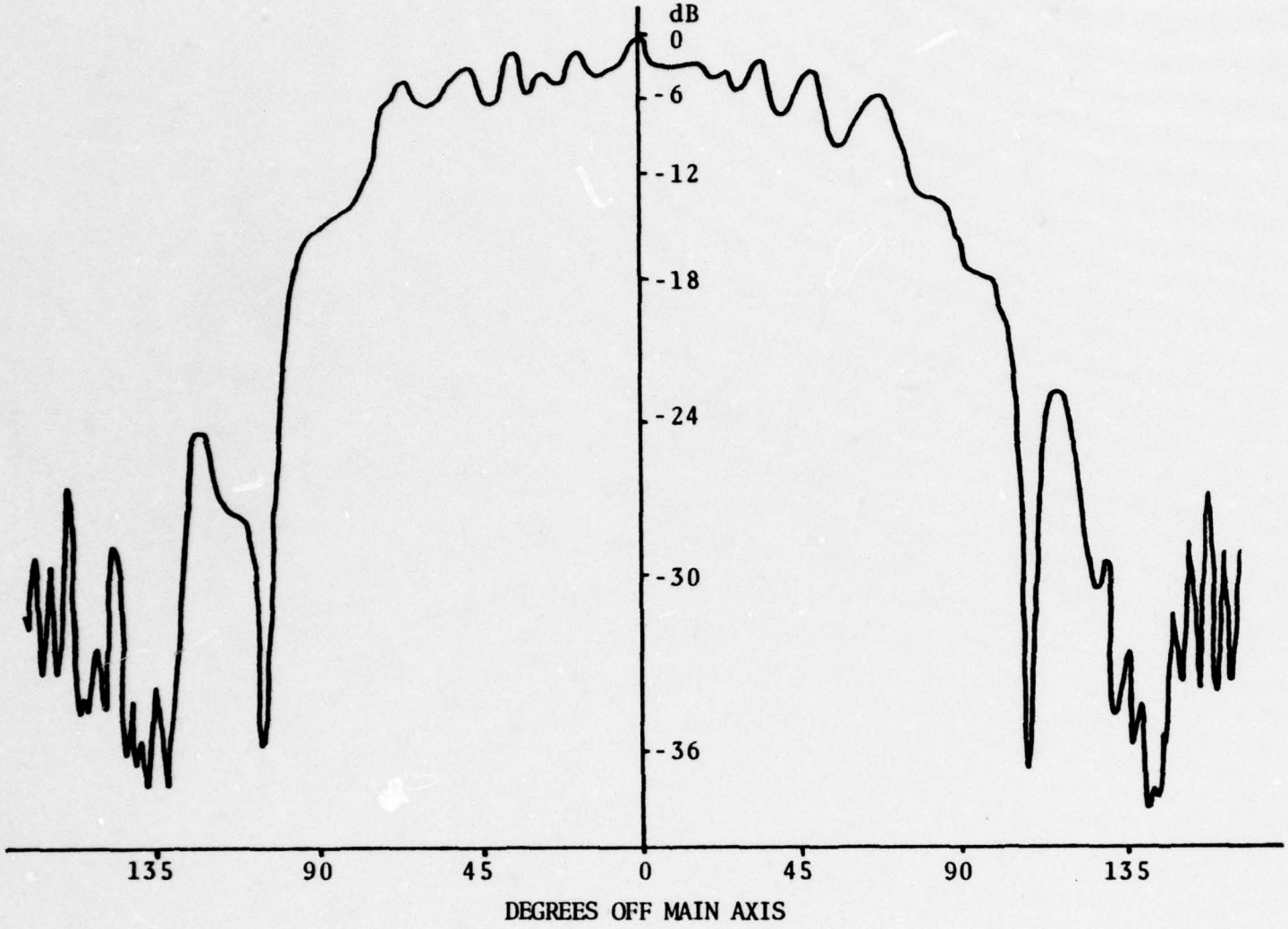

Figure 16. Radiation Pattern - 30 kHz/32 Cycle Pulse.

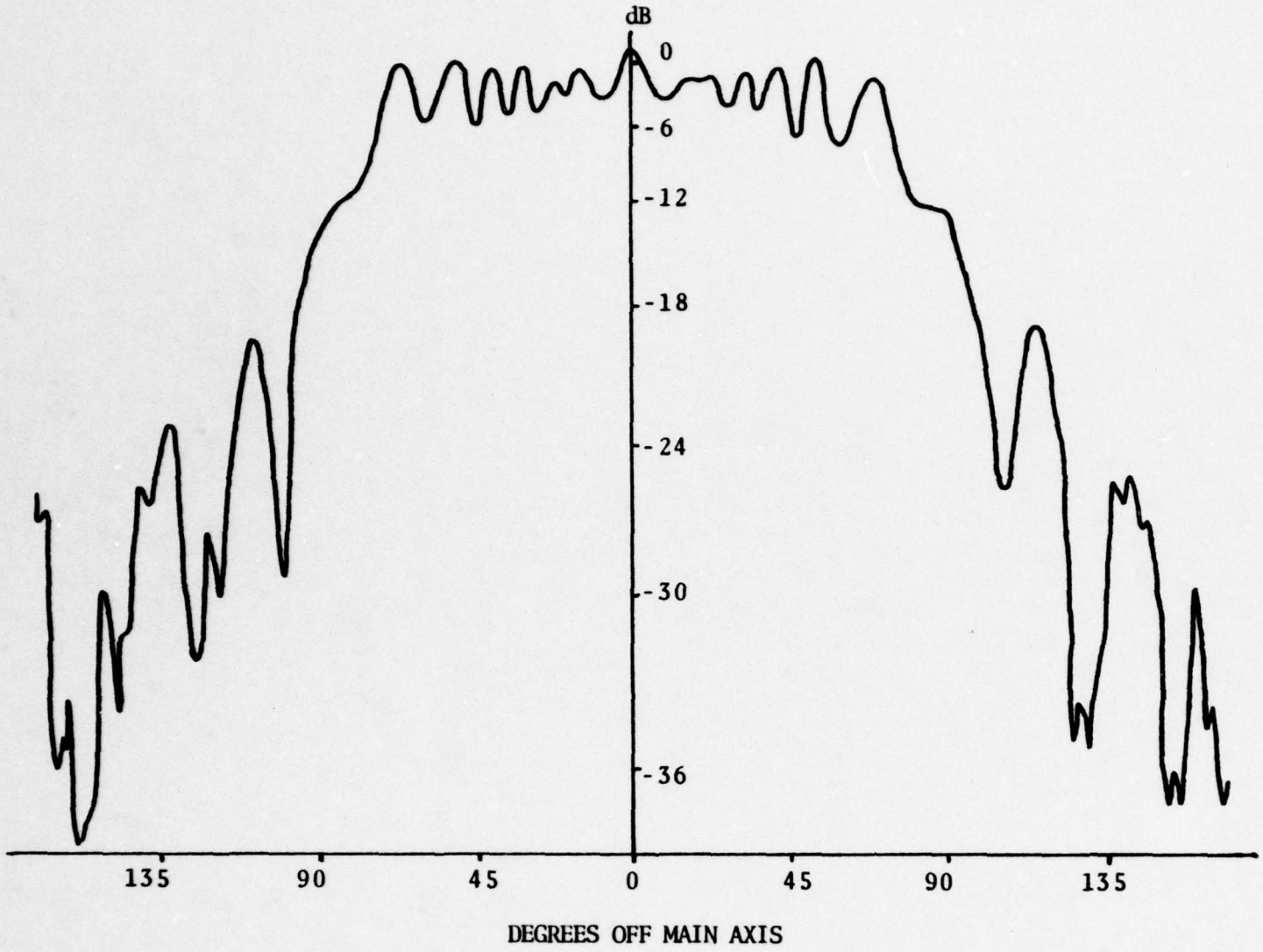

Figure 17. Radiation Pattern - 35 kHz/32 Cycle Pulse

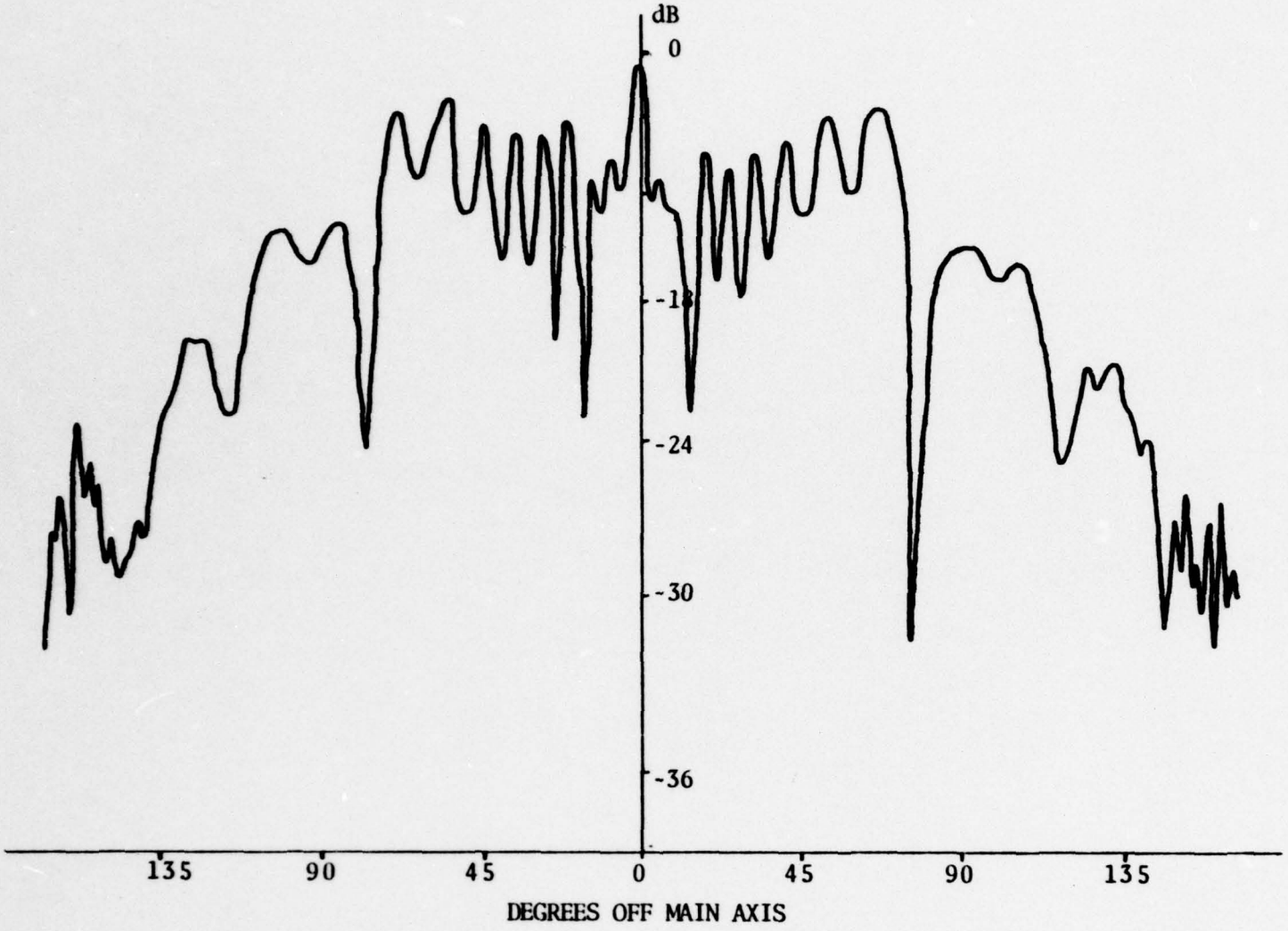

Figure 18. Radiation Pattern - 40 kHz/32 Cycle Pulse

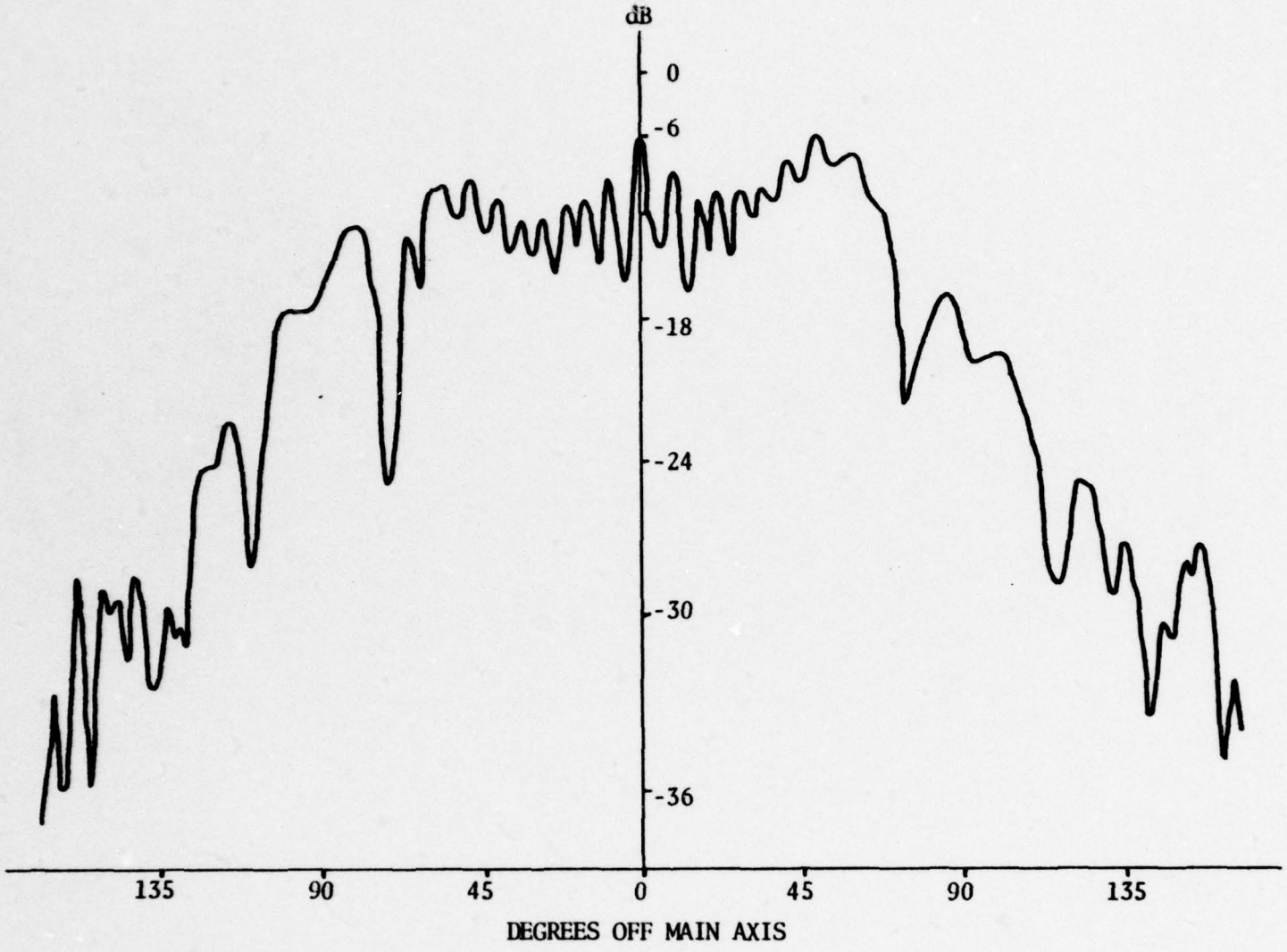

Figure 19. Radiation Pattern - 45 kHz/32 Cycle Pulse

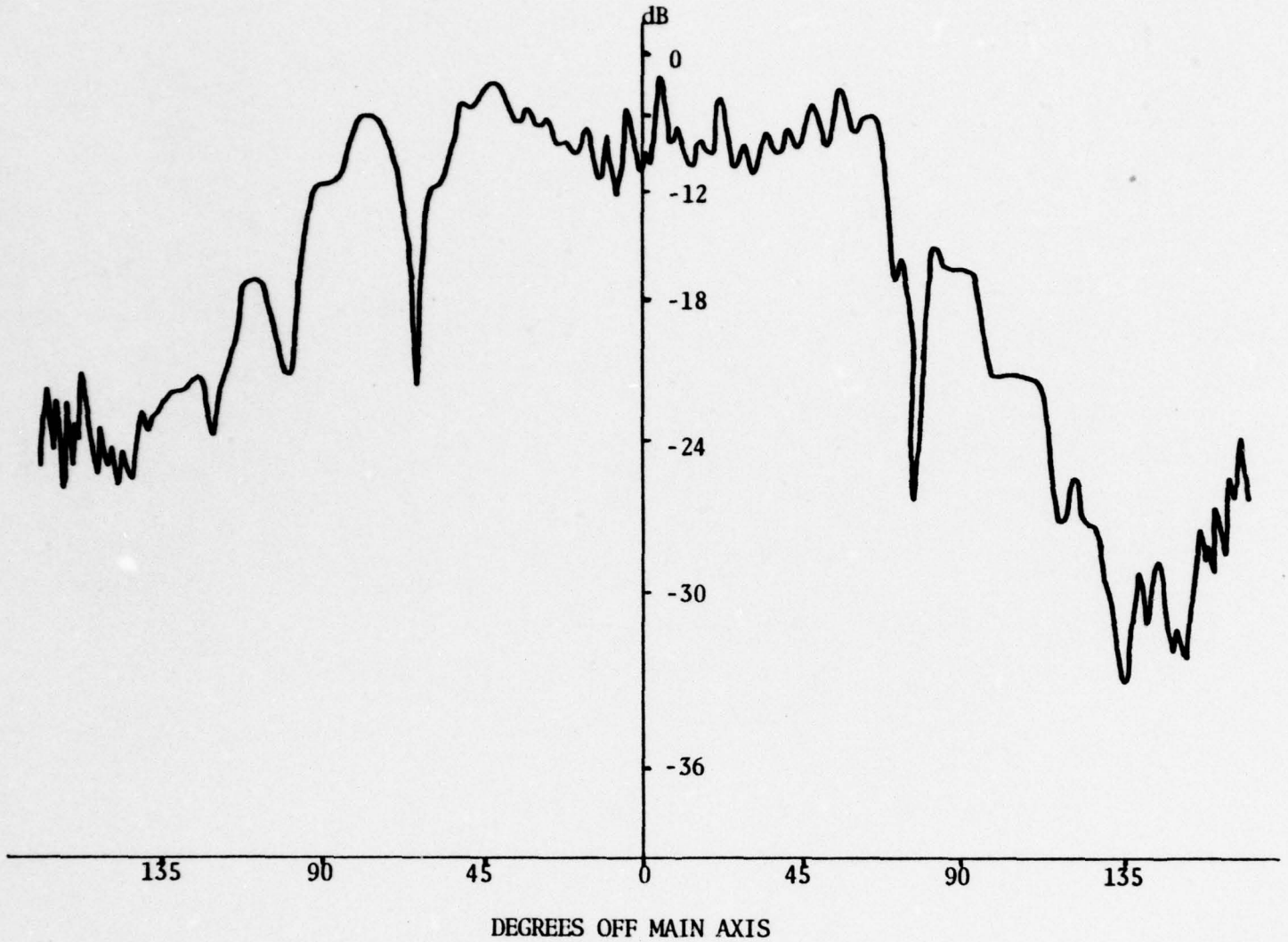

Figure 20. Radiation Pattern - 50 kHz/32 Cycle Pulse

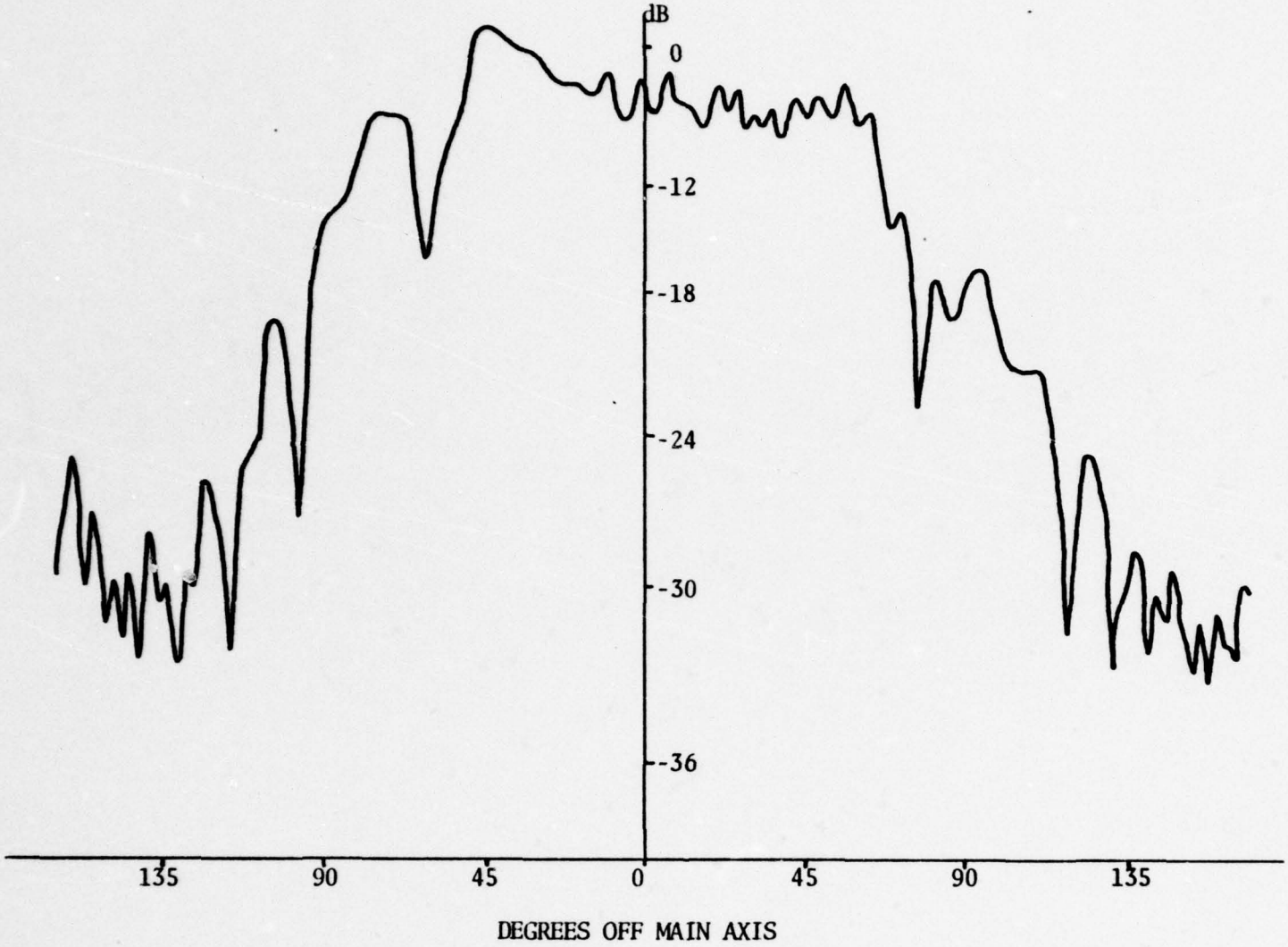

Figure 21. Radiation Pattern - 55 kHz/32 Cycle Pulse

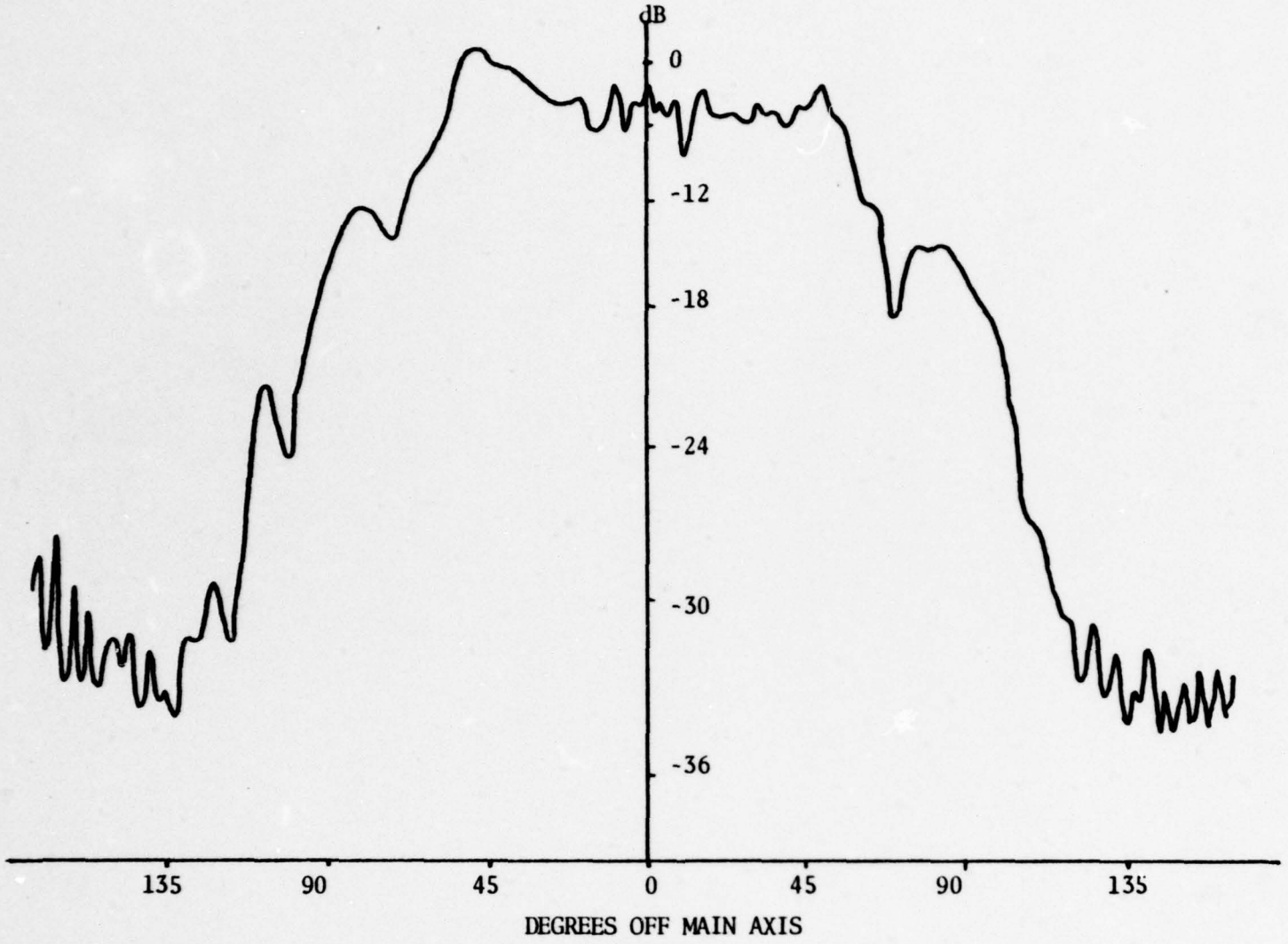

Figure 22. Radiation Pattern - 60 kHz/32 Cycle Pulse

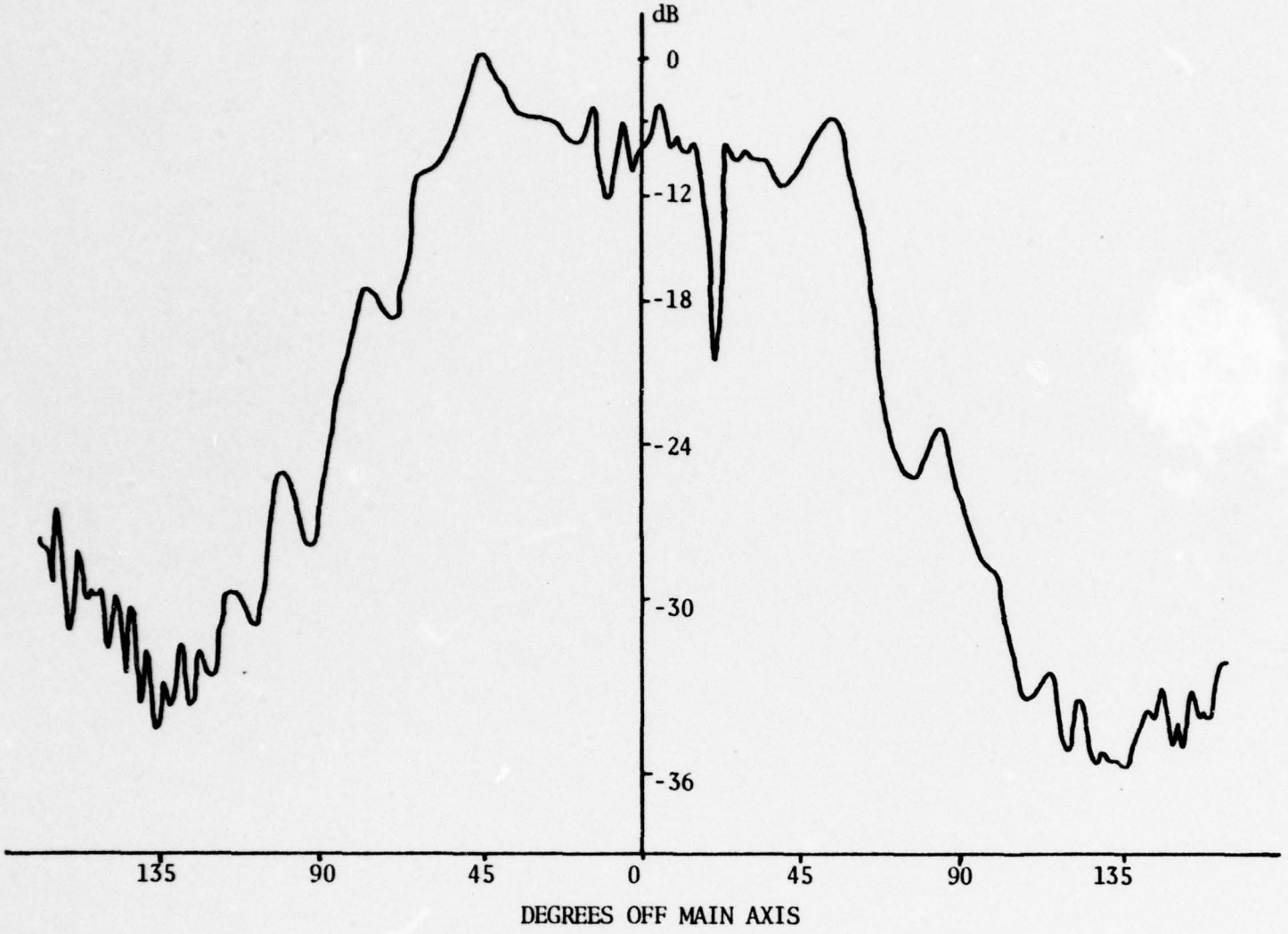

Figure 23. Radiation Pattern - 65 kHz/32 Cycle Pulse

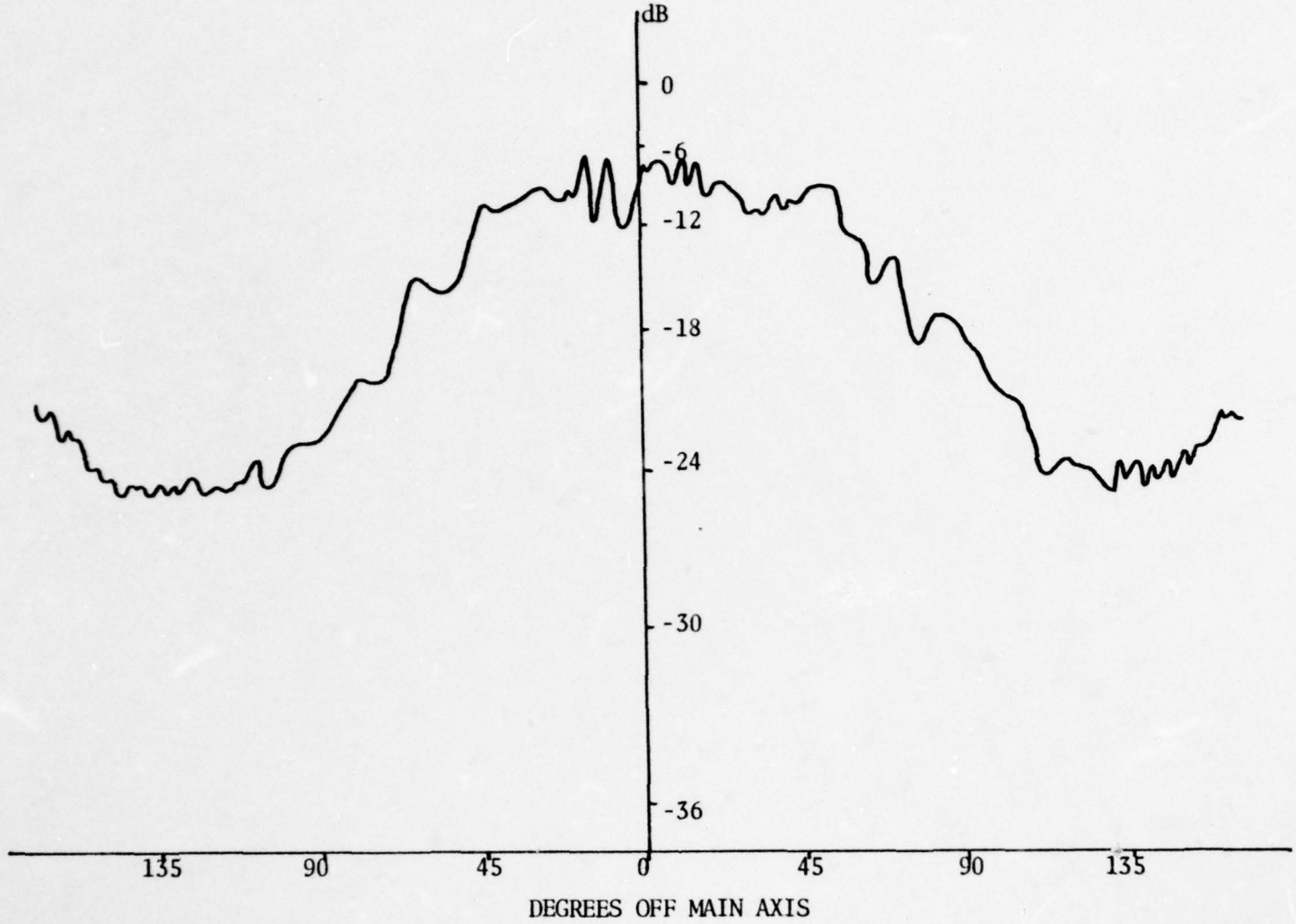

Figure 24. Radiation Pattern - 70 kHz/32 Cycle Pulse

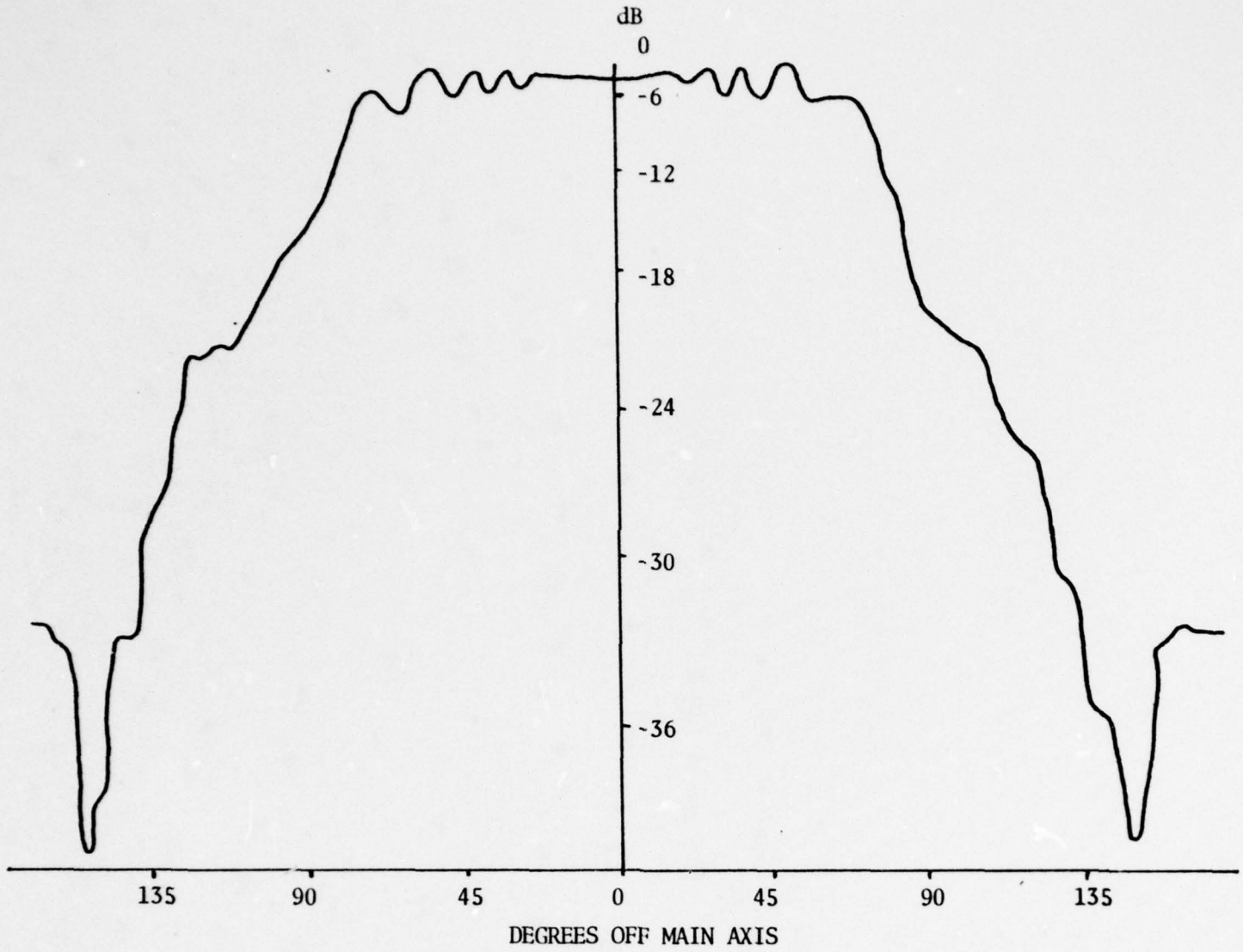

Figure 25. Radiation Pattern - 30 kHz/4 Cycle Pulse

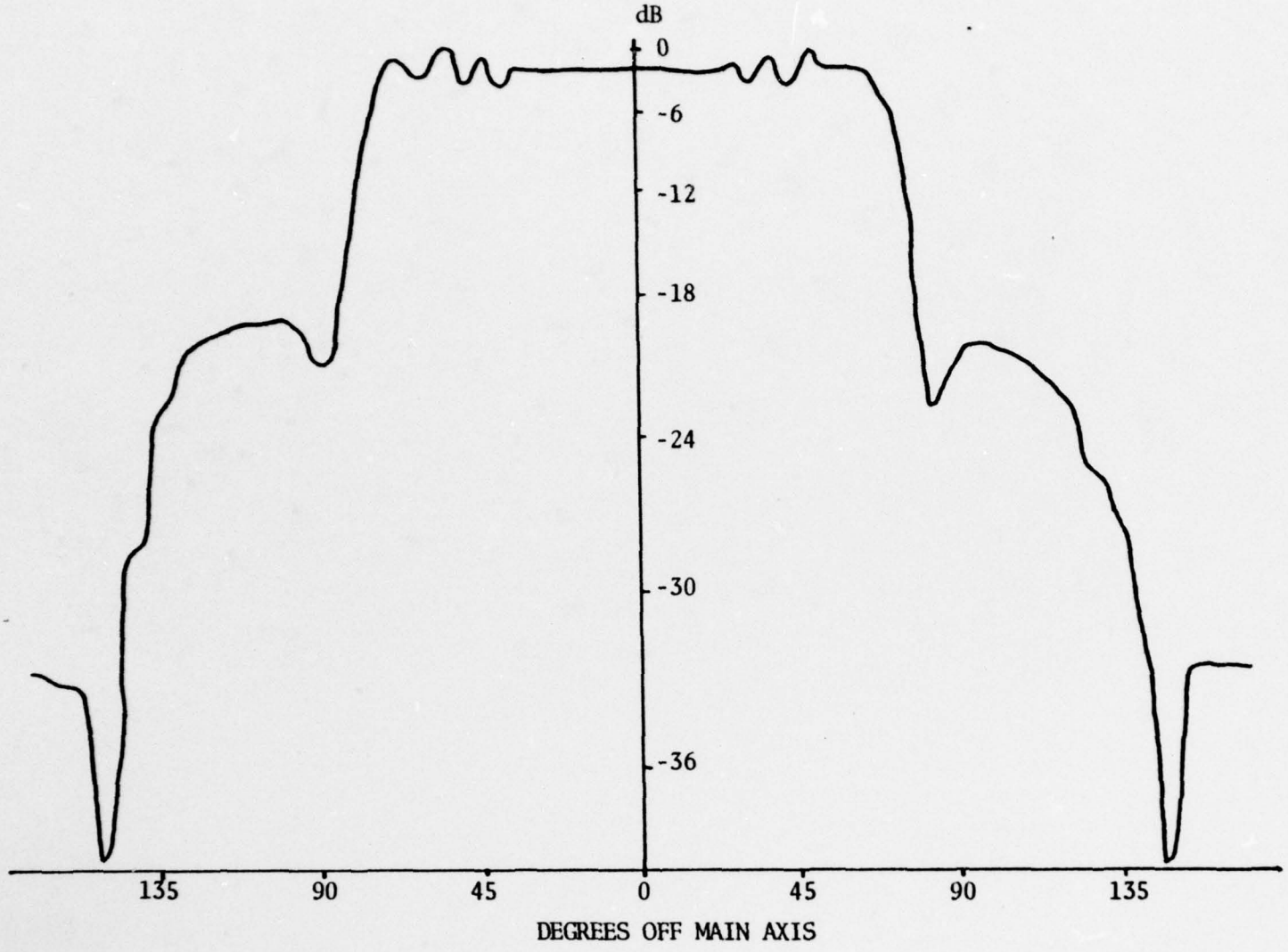

Figure 26. Radiation Pattern - 35 kHz/4 Cycle Pulse

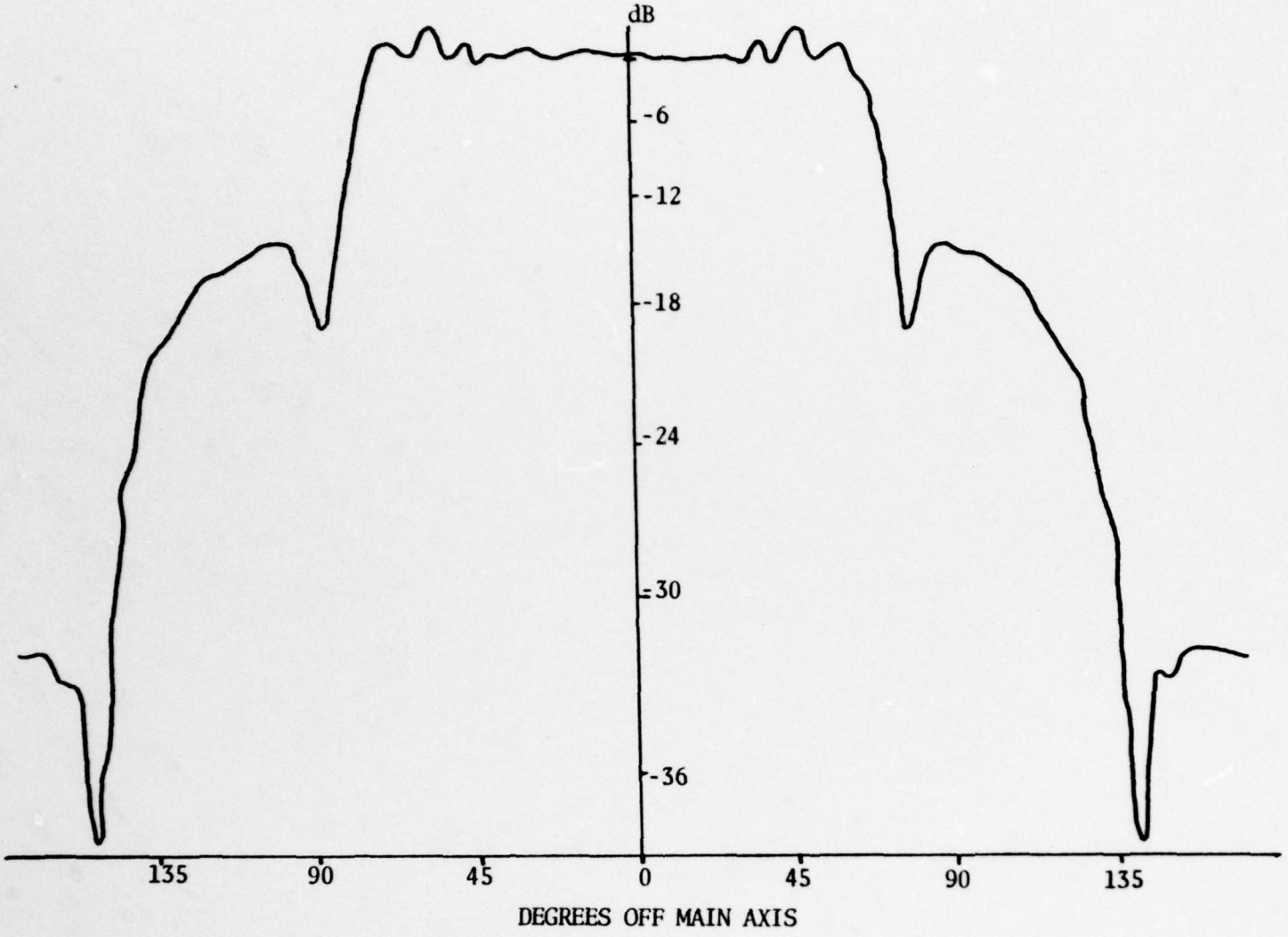

Figure 27. Radiation Pattern - 40 kHz/4 Cycle Pulse

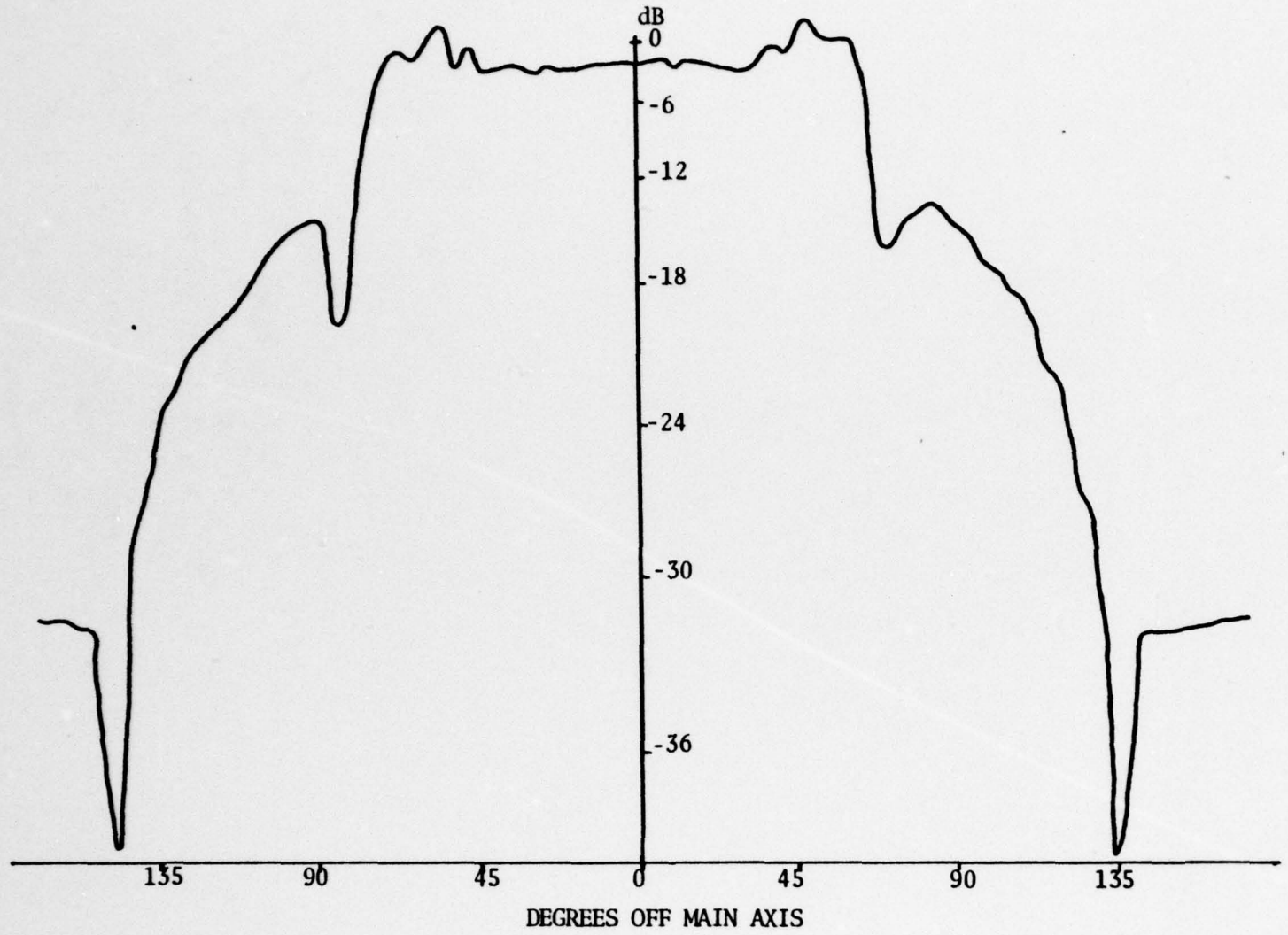

Figure 28. Radiation Pattern - 45 kHz/4 Cycle Pulse

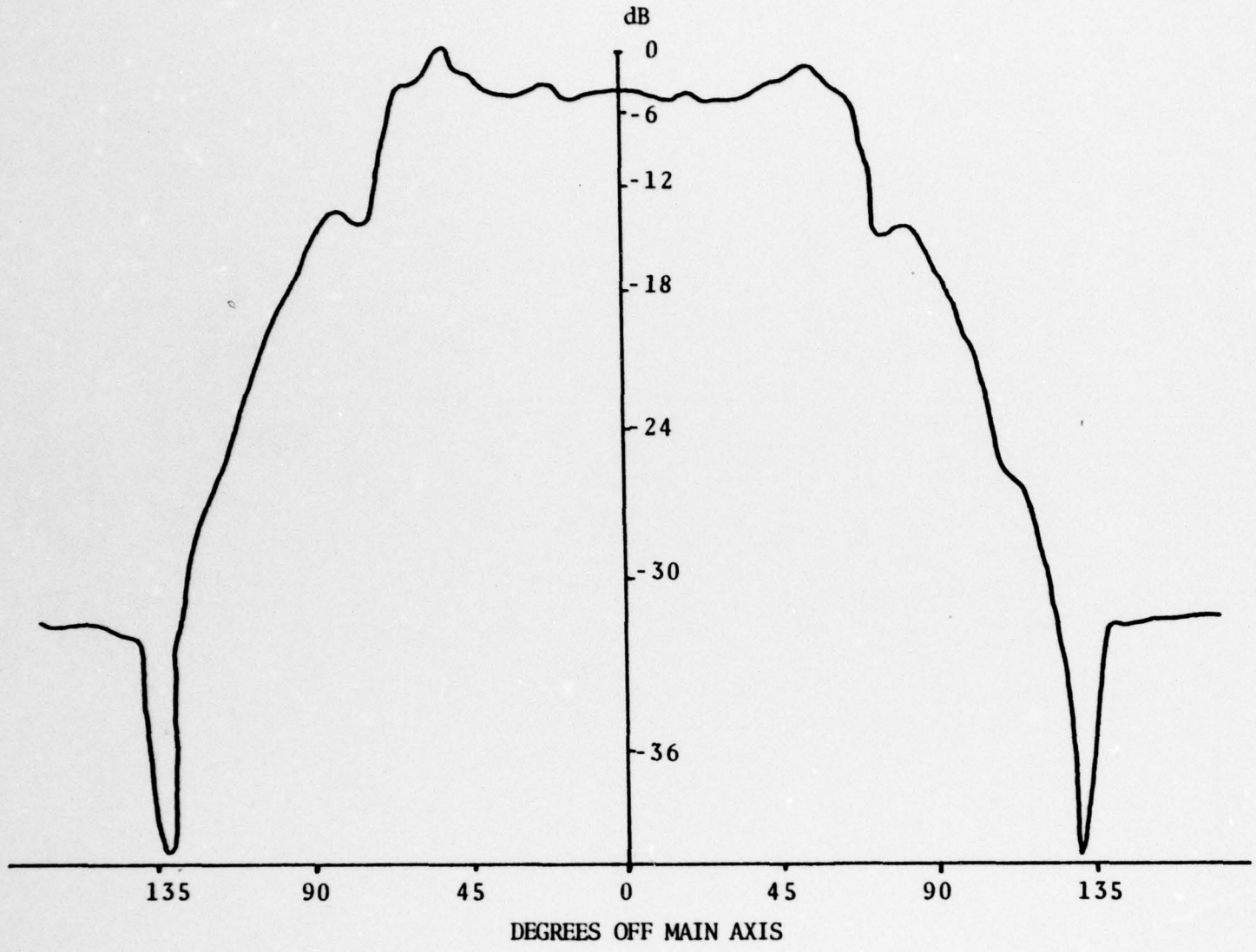

Figure 29. Radiation Pattern - 50 kHz/4 Cycle Pulse

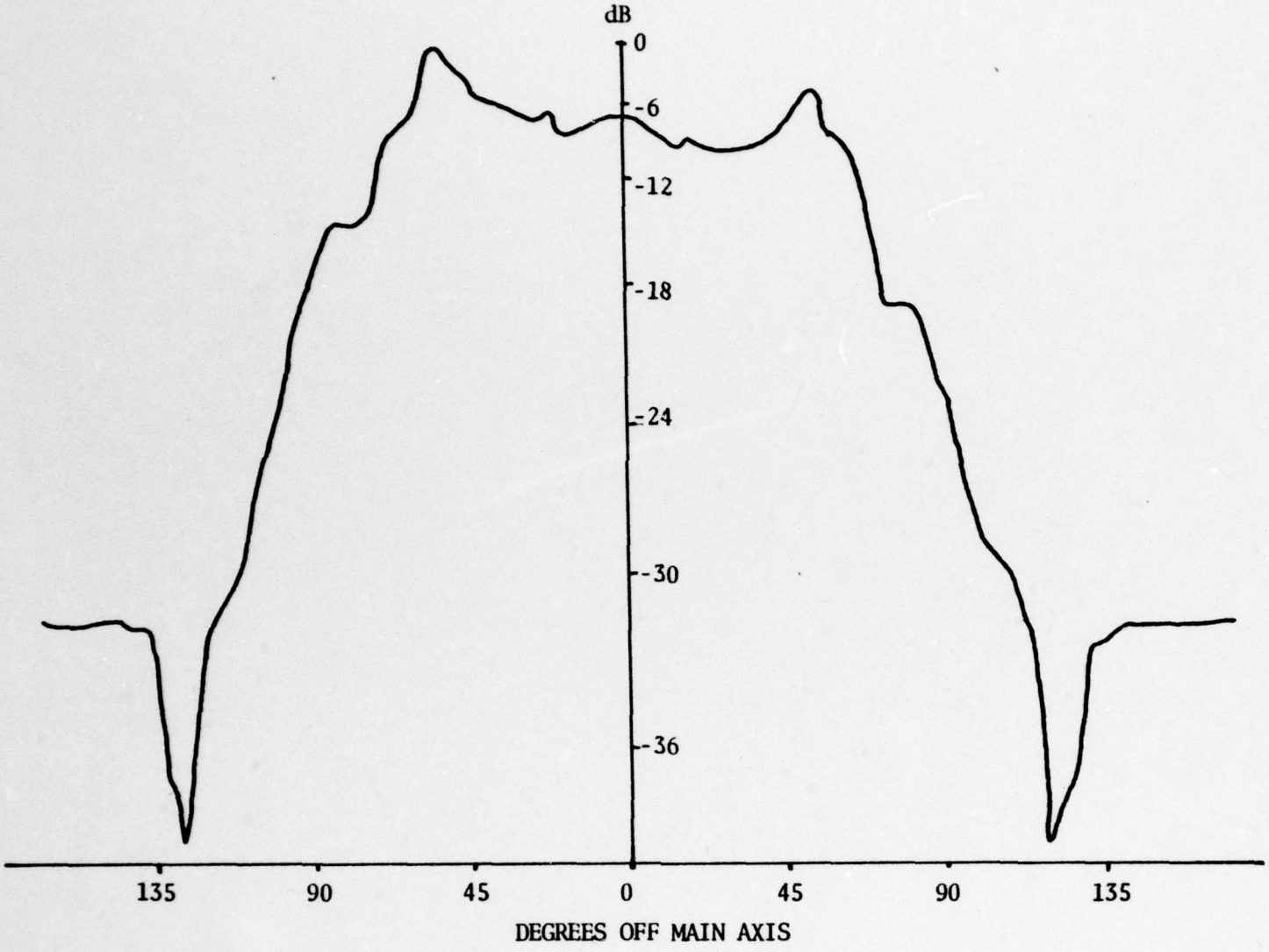

Figure 30. Radiation Pattern - 55 kHz/4 Cycle Pulse

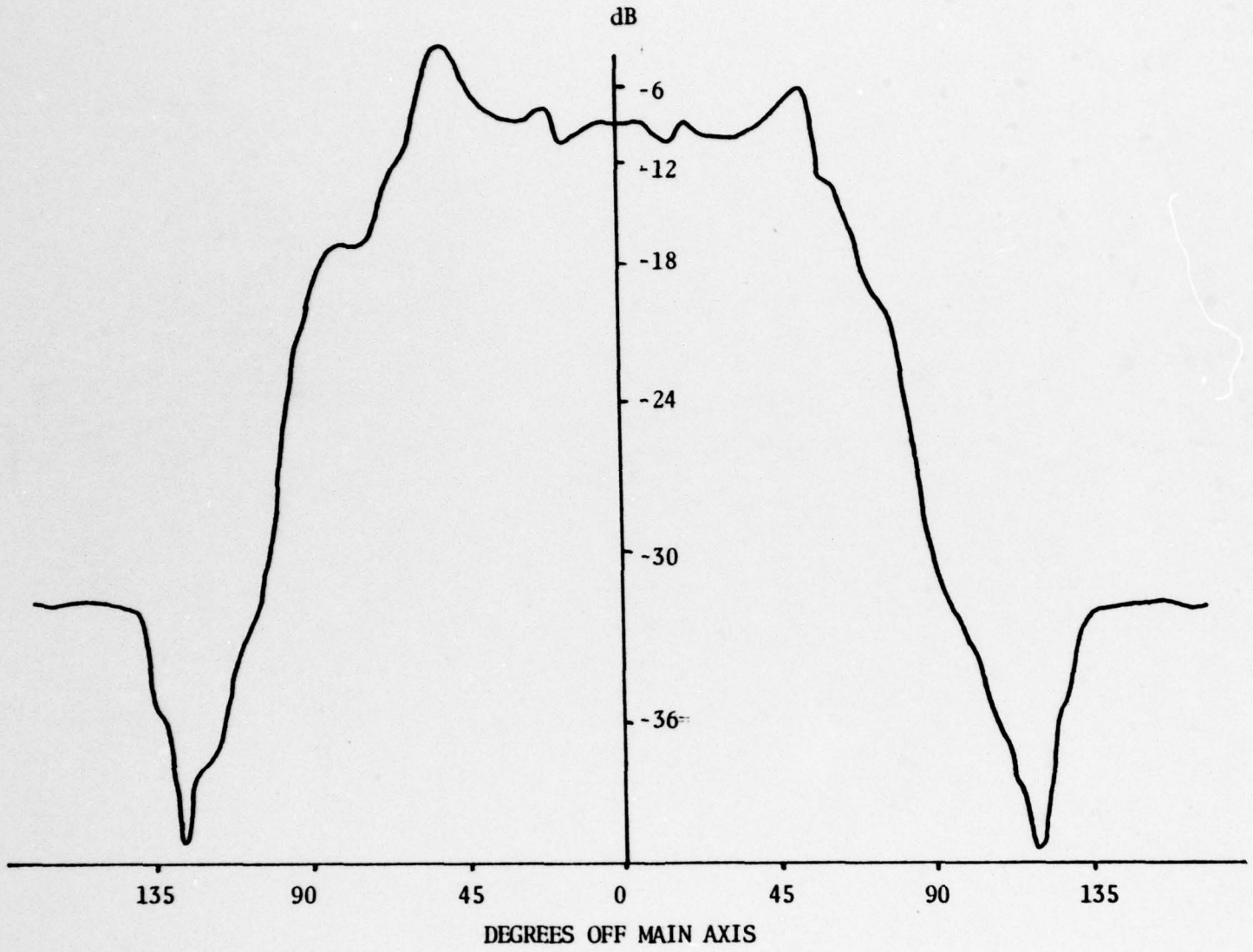

Figure 31. Radiation Pattern - 60 kHz/4 Cycle Pulse

TABLE V

BEAM PATTERN MEASUREMENT EQUIPMENT PARAMETERS

	Figure	Frequency (kHz)	No. of Cycles	Pulse Length (microsec)	Gate Width (microsec)
SET A.	16	30	32	1067	500
	17	35	32	914	500
	18	40	32	800	500
	19	45	32	711	500
	20	50	32	640	500
	21	55	32	581	500
	22	60	32	533	500
	23	65	32	492	500
	24	70	32	457	300
SET B.	25	30	4	133	130
	26	35	4	114	100
	27	40	4	100	100
	28	45	4	89	80
	29	50	4	80	80
	30	55	4	73	70
	31	60	4	67	60

The first set of radiation patterns was made using a 32-cycle pulse. This was the longest pulse that could be used without having the water-air surface reflected signal interfere with the direct path signal at 30 kHz. The boxcar integrator gatewidth was maintained at 500 μsec. The only discernable feature from this first set of radiation patterns is the highly variable amplitude. By making nearfield measurements at a distance of one centimeter from the plate, it was found that the plate radiated more strongly from the center region of the plate and from the edge region of the plate. This effect, combined with the large radius (31.75 cm) of the plate, resulted in the large amplitude variations as the plate rotated. To eliminate the interference effects of the waves arriving from the edge region of the plate, a short (4 cycle) pulse was used. This permitted separating the waves arriving from the central portion and edge region of the plate by properly gating the boxcar integrator. By reducing the edge effects, a closer approximation was obtained to the infinite plate used in Feit's theory. As can be seen, most of the interference effects are eliminated and the radiation patterns are much smoother. Starting at 45 kHz (Fig. 28), the radiation patterns change from a relatively flat, broad, single lobe to two side lobes approximately 60 degrees off the plate axis at 60 kHz. This is in qualitative agreement with Feit's calculations for the infinite fluid-loaded plate.

IV. DISCUSSION OF RESULTS

Because all of the experimental work was done with a single plate, it was impossible to arrive at general conclusions. For the data obtained in air, good agreement was obtained with the Mindlin-Timoshenko plate theory for the speed of the flexural wave as a function of frequency. In comparing the in-water data with the in-air data, the flexural-wave speed with water loading is approximately 11 percent lower than with air loading at 15 kHz and approximately 14 percent lower at 45 kHz. Plate natural frequencies were 18 percent lower for both the tenth and eighteenth axisymmetric modes, occurring in air at 14931 Hz and 40949 Hz, respectively. These results agree qualitatively with theory. Additionally, the changes which occur in the radiation patterns above 45 kHz, which is approximately the critical frequency for the plate, appear to agree qualitatively with Feit's theory for the infinite fluid-loaded plate.

The most significant effect noted, which is not predicted by any of the theory reviewed by the author, is the behavior of the flexural-wave speed above the critical frequency. Although different measurement techniques were used to obtain the data, there is an indication of a significant (15 percent) increase in flexural wave speed occurring in the vicinity of 45 kHz. It is in this frequency range that the experimental data for flexural-wave speed approaches the speed of sound

in water. Although the possibility exists that different experimental techniques caused this result, the two methods of obtaining data agreed within five percent at frequencies below the critical frequency and repeated observations indicate that the result is real. There is clearly a change in the radiation resistance as frequency increases, as evidenced by the increased damping of the plate natural frequencies with increasing frequency. At frequencies below the critical frequency, the fluid adds inertia which causes a lower flexural wave speed. If this effect is real, it indicates that the radiation reactance (inertial) becomes much smaller above the critical frequency.

V. RECOMMENDATIONS

The results of this work and those of Sevdik are a promising indication of the feasibility of using a flexural disk transducer as a high-frequency, broad-beam sound source. Other advantages of a flexural disk transducer are its simplicity of construction, ruggedness, and adaptability for flush mounting or as part of the hull structure of the vehicle in which it is used.

An in-depth theoretical study leading to a working model transducer, following the theory contained in the Alper-Magrab paper, is recommended. The effects of shear and rotatory inertia are significant at the frequencies in question and must be considered. This work and the theory presented by Feit indicate that significant changes in radiation patterns do occur at frequencies above the critical frequency. Further investigation into these changes and the possible changes in flexural wave speed observed in this work are recommended.

APPENDIX A

COMPARISON OF NODAL CIRCLE SPACING WITH FLEXURAL WAVELENGTH

From Leissa [Ref. 7, p. 11], substituting Ω^2 for Leissa's λ^2,

$$\Omega^2 = \omega a^2 \left[\frac{m}{D}\right]^{1/2} = \omega a^2 \left[\frac{\rho h}{D}\right]^{1/2} \tag{A-1}$$

From classical plate theory [Ref. 4, p. 44],

$$C^2 = \frac{D}{\rho h}\left(\frac{2\pi}{\lambda}\right)^2 \tag{A-2}$$

Rearranging (A-2)

$$D = C^2 \rho h \left(\frac{\lambda}{2\pi}\right)^2 \tag{A-3}$$

Substituting for D in (A-1) using (A-3)

$$\Omega^2 = \frac{2\pi \omega a^2}{C\lambda} \tag{A-4}$$

Substituting $\omega = 2\pi f$ and $c = f\lambda$ into (A-4)

$$\Omega^2 = \frac{4\pi^2 a^2}{\lambda^2} \tag{A-5}$$

Rearranging (A-5)

$$\frac{\lambda}{a} \quad \frac{2\pi}{\sqrt{\Omega^2}} \tag{A-6}$$

Where Ω^2 is obtained from Leissa [Ref. 7, Table 2.5].

From Leissa [Ref. 7, Table 2.7], the spacing between nodal circles for a free-edge, circular plate with Poisson's ratio equal to 0.33 equals 0.200 r/a, for the 5,0 mode, where r is the distance from the center of the plate to the nodal circle and a is the plate radius.

Assuming the spacing between nodal circles is one-half flexural wavelength, for the 5,0 mode, $\lambda = 0.400a$. Using $\Omega^2 = 245.9$ (Table 2.5 for the 5,0 mode) to substitute into equation A-6,

$$\lambda = \frac{2\pi a}{\sqrt{245.9}} = 0.401a$$

For the 5,0 mode, classical plate theory gives a value of $\lambda = 0.401a$ when solving from calculated eigenvalues and 0.400 when solving using nodal circle spacing.

LIST OF REFERENCES

1. Sevdik, Omer, Development of a Flexural Disk Transducer for Acoustic Tracking of Underwater Vehicles, M.S. Thesis, Naval Postgraduate School, Monterey, 1976.

2. Morse, Philip M. and Ingard, Uno K., Theoretical Acoustics, p. 213-219, McGraw-Hill, 1968.

3. Malecki, I., Physical Foundations of Technical Acoustics, p. 505-509, Pergamon Press, 1969.

4. Mindlin, R. D., "Influence of Rotatory Inertia and Shear on Flexural Motions of Isotropic, Elastic Plates," Journal of Applied Mechanics, v. 18, p. 31-38, March 1951.

5. Alper, Stanley and Magrab, Edward B., "Radiation from the Forced Harmonic Vibrations of a Clamped Circular Plate in an Acoustic Fluid," The Journal of the Acoustical Society of America, v. 48, Number 3 (Part 2), p. 681-691, 1970.

6. Feit, David, "Pressure Radiated by a Point-Excited Elastic Plate," The Journal of the Acoustical Society of America, v. 40, Number 6, p. 1489-1494, 1966.

7. Leissa, Arthur W., Vibration of Plates, NASA SP-160, p. 1-11, National Aeronautics and Space Administration, 1969.

8. Rayleigh, Lord, Theory of Sound, v. I, p. 251-252, Dover, The MacMillan Co., 1945 (originally published in 1877).

9. Timoshenko, S., "On the Correction for Shear of the Differential Equations for Transverse Vibrations of Prismatic Bars," Philosophical Magazine, Ser. 6, v. 41, p. 742, 1921.

10. Kinsler, Lawrence E. and Frey, Austin R., Fundamentals of Acoustics, p. 502, Wiley, 1950.

INITIAL DISTRIBUTION LIST

		No. Copies
1.	Defense Documentation Center Cameron Station Alexandria, Virginia 22314	2
2.	Library, Code 0212 Naval Postgraduate School Monterey, California 93940	2
3.	Department Chairman, Code 61 Department of Physics and Chemistry Naval Postgraduate School Monterey, California 93940	1
4.	Professor O. B. Wilson, Code 61 W1 Department of Physics and Chemistry Naval Postgraduate School Monterey, California 93940	5
5.	Department Library, Code 61 Department of Physics and Chemistry Naval Postgraduate School Monterey, California 93940	1
6.	Mr. R. L. Marimon, Code 7000 Naval Torpedo Station Keyport, Washington 98345	2
7.	Mr. Michael L. Barlow, Code 7042 Naval Torpedo Station Keyport, Washington 98345	1
8.	LCDR James L. Jarvis COMIDEAST FOR STAFF FPO New York, N.Y. 09501	1